Draft version August 29, 2018
Preprint typeset using LATEX style emulateapj v. 08/13/06

OISTER OPTICAL AND NEAR-INFRARED OBSERVATIONS OF TYPE IAX SUPERNOVA 2012Z

Masayuki Yamanaka[1,2,3,4], Keiichi Maeda[5,6], Koji S. Kawabata[3], Masaomi Tanaka[7],
Nozomu Tominaga[1,6], Hiroshi Akitaya[3], Takahiro Nagayama[8,9], Daisuke Kuroda[10],
Jun Takahashi[11], Yoshihiko Saito[12], Kenshi Yanagisawa[10], Akihiko Fukui[10],
Ryo Miyanoshita[9], Makoto Watanabe[13], Akira Arai[11,14], Mizuki Isogai[7,14],
Takashi Hattori[15], Hidekazu Hanayama[16], Ryosuke Itoh[4], Takahiro Ui[4],
Katsutoshi Takaki[4], Issei Ueno[4], Michitoshi Yoshida[3], Gamal B. Ali[17],
Ahmed Essam[17], Akihito Ozaki[13], Hikaru Nakao[13], Ko Hamamoto[13],
Daisaku Nogami[2,5], Tomoki Morokuma[18], Yumiko Oasa[19],
Hideyuki Izumiura[10], and Kazuhiro Sekiguchi[7].

Draft version August 29, 2018

ABSTRACT

We report observations of the Type Iax supernova (SN Iax) 2012Z at optical and near-infrared wavelengths from immediately after the explosion until ~ 260 days after the maximum luminosity using the Optical and Infrared Synergetic Telescopes for Education and Research (OISTER) Target-of-Opportunity (ToO) program and the Subaru telescope. We found that the near-infrared (NIR) light curve evolutions and color evolutions are similar to those of SNe Iax 2005hk and 2008ha. The NIR absolute magnitudes ($M_J \sim -18.1$ mag and $M_H \sim -18.3$ mag) and the rate of decline of the light curve ($\Delta\,m_{15}(B) = 1.6 \pm 0.1$ mag) are very similar to those of SN 2005hk ($M_J \sim -17.7$ mag, $M_H \sim -18.0$ mag, and $\Delta\,m_{15}(B) \sim 1.6$ mag), yet differ significantly from SNe 2008ha and 2010ae ($M_J \sim -14 - -15$ mag and $\Delta\,m_{15}(B) \sim 2.4 - 2.7$ mag). The estimated rise time is 12.0 ± 3.0 days, which is significantly shorter than that of SN 2005hk or any other Ia SNe. The rapid rise indicates that the ^{56}Ni distribution may extend into the outer layer or that the effective opacity may be lower than that in normal SNe Ia. The late-phase spectrum exhibits broader emission lines than those of SN 2005hk by a factor of 6–8. Such high velocities of the emission lines indicate that the density profile of the inner ejecta extends more than that of SN 2005hk. We argue that the most favored explosion scenario is a 'failed deflagration' model, although the pulsational delayed detonations is not excluded.

Subject headings: supernovae: general — supernovae: individual (SN 2012Z) — supernovae: individual (SNe 2005hk)

1. INTRODUCTION

Type Ia supernovae (SNe Ia) provide a strong constraint on the cosmological parameters (Riess et al. 1998; Perlmutter et al. 1999) because their peak luminosities are well correlated with the widths of their light curves (Pskovskii 1984; Phillips 1993; Phillips et al. 1999; Altavilla et al. 2004; Wang et al. 2005, 2006; Prieto et al. 2006; Jha et al. 2007; Conley et al. 2008; Folatelli et al. 2010). More luminous objects typically have slower rates of decline of their light curves. However, although normal SNe Ia exhibit such homogeneous properties, various diverse properties have recently been discovered, e.g., SNe Iax (Li et al. 2003; Phillips et al. 2007; Valenti et al. 2009), super-Chandrasekhar SNe (Howell et al. 2006; Hicken et al. 2007; Yamanaka et al. 2009a), and SNe Ia/IIn (Hamuy et al. 2003; Aldering et al. 2006).

SNe Iax are one of the most mysterious SNe (Li et al. 2003; Phillips et al. 2007; Sahu et al. 2008; Valenti et al. 2009; Foley et al. 2010a,b; Narayan et al. 2011; Stritzinger et al. 2014; White et al. 2015). The peak lu-

[1] Department of Physics, Faculty of Science and Engineering, Konan University, Okamoto, Kobe, Hyogo 658-8501, Japan; yamanaka@center.konan-u.ac.jp
[2] Kwasan Observatory, Kyoto University, 17-1 Kitakazan-ohmine-cho, Yamashina-ku, Kyoto, 607-8471
[3] Hiroshima Astrophysical Science Center, Hiroshima University, Higashi-Hiroshima, Hiroshima 739-8526, Japan
[4] Department of Physical Science, Hiroshima University, 1-3-1 Kagamiyama, Higashi-Hiroshima 739-8526, Japan
[5] Department of Astronomy, Graduate School of Science, Kyoto University, Sakyo-ku, Kyoto 606-8502, Japan
[6] Institute for the Physics and Mathematics of the Universe (WPI), University of Tokyo, Kashiwa, Japan
[7] National Astronomical Observatory of Japan, 2-21-1 Osawa, Mitaka, Tokyo 181-8588, Japan
[8] Department of Astrophysics, Nagoya University, Chikusa-ku, Nagoya 464-8602, Japan
[9] Graduate School of Science and Engineering, Kagoshima University, 1-21-35 Korimoto, Kagoshima 890-0065, Japan
[10] Okayama Astrophysical Observatory, National Astronomical Observatory of Japan, 3037-5 Honjo, Kamogata, Asakuchi, Okayama 719-0232, Japan
[11] Nishi-Harima Astronomical Observatory, Center for Astronomy, University of Hyogo, 407-2 Nishigaichi, Sayo-cho, Sayo, Hyogo 679-5313, Japan
[12] Department of Physics, Tokyo Institute of Technology, 2-12-1 Ookayama, Meguro-ku, Tokyo 152-8551, Japan
[13] Department of Cosmosciences, Hokkaido University, Kita 10, Nishi 8, Kita-ku, Sapporo, Hokkaido 060-0810, Japan
[14] Koyama Astronomical Observatory, Kyoto Sangyo University, Motoyama, Kamigamo, Kita-Ku, Kyoto-City 603-8555, Japan
[15] Subaru Telescope, 650 North Aohoku Place, Hilo, HI 96720, USA
[16] Ishigakijima Astronomical Observatory, National Astronomical Observatory of Japan, 1024-1 Arakawa, Ishigaki, Okinawa 907-0024, Japan
[17] National Research Institute of Astronomy and Geophysics, Cairo 11722, Egypt
[18] Institute of Astronomy, Graduate School of Science, The University of Tokyo, 2-21-1 Osawa, Mitaka, Tokyo 181-0015, Japan
[19] Faculty of Education, Saitama University, 255 Shimo-Okubo, Sakura, Saitama, 338-8570, Japan

arXiv:1505.01593v2 [astro-ph.SR] 11 May 2015

minosities are significantly fainter than those expected from the rates of decline of their light curves. Their light curves do not exhibit a secondary maximum in the I band 20–30 days after the B-band maximum, and their spectra exhibit a blue continuum with absorption lines for ions in relatively high ionization states during the early phases, e.g., Fe III rather than Si II (Branch et al. 2004). The line velocity exhibits a diversity from 2000 to 8000 km s^{-1} among SNe Iax. These velocities are significantly lower than those of normal SNe Ia (Foley et al. 2013).

There is no comprehensive explosion model to describe the observed properties of SNe Iax. The small line velocities suggest that the explosion energy could be much smaller than for normal SNe Ia. Phillips et al. (2007) proposed a pure deflagration model (Nomoto et al. 1984) to describe these observed properties. With a pure deflagration model, strong mixing is expected to occur due to hydrodynamic instabilities (Gamezo et al. 2003). Such mixing could result in a singly peaked light curve in the near-infrared (NIR) (Blinnikov et al. 2006). Alternatively, a core collapse scenario has also been proposed to describe extremely faint SNe Iax (Moriya et al. 2010).

A progenitor candidate of SNe Iax has been searched for in pre-explosion images (Foley et al. 2010b; McCully et al. 2014). For SN 2012Z, a blue source was detected in the pre-explosion images taken using the *Hubble Space Telescope* (*HST*) (McCully et al. 2014). The luminosity ($M_V \sim -5.3$ mag) and color were similar to those of an He star or a quiescent phase of the helium nova V445 Pup (Kamath & Anupama 2002; Iijima & Nakanishi 2008). Although He I emission lines have been reported for a few SNe Iax, spectra of SNe Iax do not necessarily exhibit He features (Jha et al. 2007; Foley et al. 2013).

SN 2012Z was discovered at an unfiltered magnitude of 17.6 mag on Jan 29.15 UT ($t = -10.65$ d [20]) by Lick Observatory Supernova Search (LOSS; Filippenko et al. 2001) in the nearby galaxy NGC 1309 (Cenko et al. 2012c). Cenko et al. (2012b) reported a follow-up photometric observation three minutes after discovery. They found that the magnitude of SN 2012Z was $V = 18.00 \pm 0.16$ mag. The spectrum was very similar to that of the luminous-class SN Ia 1991T or the well-studied SN Iax 2005hk (Cenko et al. 2012a; Meyer et al. 2012). Table 1 lists a summary of the parameters of SN 2012Z.

In this paper, we describe continuous photometric observations in NIR bands as well as optical ones. Such wide-wavelength observations of SNe Iax are rare (Phillips et al. 2007; Stritzinger et al. 2014). We focus on the NIR properties and the rise time; in particular, we show a detailed comparison with the bright SN Iax 2005hk ($M_V \sim -18.1$ mag; Phillips et al. 2007; Sahu et al. 2008), as well as the faint SNe Iax 2008ha ($M_V \sim -14.2$ mag; Valenti et al. 2009; Foley et al. 2010a) and 2010ae ($M_V \sim -14.5$ mag; Stritzinger et al. 2014). Explosion models are also discussed by comparing the expected outcomes with our observations.

2. OBSERVATIONS AND DATA REDUCTION

Observations of SN 2012Z were performed in the framework of a Target-of-Opportunity program of the Optical and Infrared Synergetic Telescopes for Education and Research (OISTER), which utilizes small ground-based telescopes in Japan, South Africa, and Chile, as part of an inter-university collaboration. The aim of OISTER is to investigate various transient sources and variable stars, including γ-ray bursts, active galactic nuclei, supernovae, and cataclysmic variables. Table 2 summarizes the instruments, telescopes, and observatories used for the observations of SN 2012Z.

2.1. NIR photometric observations

We performed J, H, and K_s-band photometric observations using the Wide-Field Camera (WFC; Yanagisawa et al. 2014) installed on the 0.91-m telescope at the Okayama Astrophysical Observatory (OAO) on five nights; the Simultaneous three-color InfraRed Imager for Unbiased Survey (SIRIUS; Nagayama et al. 2003) installed at the 1.4-m InfraRed Survey Facility (IRSF) telescopes at the South Africa Astronomical Observatory (SAAO) on 20 nights; the Nishi-harima Infrared Camera (NIC) installed at the Cassegrain focus of the 2.0-m Nayuta telescope at the Nishi-Harima Astronomical Observatory on eight nights; the Infrared Imager and Spectrograph (ISLE; Yanagisawa et al. 2006) installed at the Cassegrain focus of the 1.88-m telescope on one night; and the InfraRed Camera (IRC) installed at the 1.0-m telescope at the Iriki Observatory on 12 nights.

The obtained data were reduced as follows according to a standard procedure for ground-based NIR photometry. The sky background was subtracted using the template sky image derived in each dithering observation set. We performed point-spread function (PSF) fitting photometry using the *DAOPHOT* package of *IRAF*.

2.2. Optical photometric observations

In addition to the NIR photometric observations, we performed B, V, R, and I-band photometric observations using the Hiroshima One-shot Wide-field Polarimeter (HOWPol; Kawabata et al. 2008) installed at the 1.5-m Kanata telescope on 26 nights, and U, B, V, R, and I-band observations with the Multi-Spectral Imager (MSI; Watanabe et al. 2012) installed at the 1.6-m Pirka telescope on four nights. We also performed g', R, and I-band observations using three robotic observations systems: the Multicolor Imaging Telescopes for Survey and Monstrous Explosions (MITSuME; Kotani et al. 2005); with MITSuME at OAO (Yanagisawa et al. 2010) on 14 nights; at the Akeno Observatory on 10 nights; and at the Ishigaki-jima Astronomical Observatory on seven nights. Adding to the OISTER collaboration, we performed B, V, R, and I-band photometric observations using the 1.88-m telescope at the Kottamia Observatory on two nights. These data were reduced according to a standard procedure for charge-coupled device (CCD) photometry. We used PSF photometry, as with the NIR data.

2.3. Optical spectroscopy

We performed optical spectroscopic monitoring using HOWPol on 12 nights, and with the low-resolution spectrograph LOSA/F2 (Shinnaka et al. 2013) mounted on the Nasmyth stage of the 1.3-m Araki telescope at the Koyama Astronomical Observatory on four nights (Table

---

[20] We adopt MJD 55965.8 ± 3.0 as $t = 0$ throughout this paper; see §3.1.
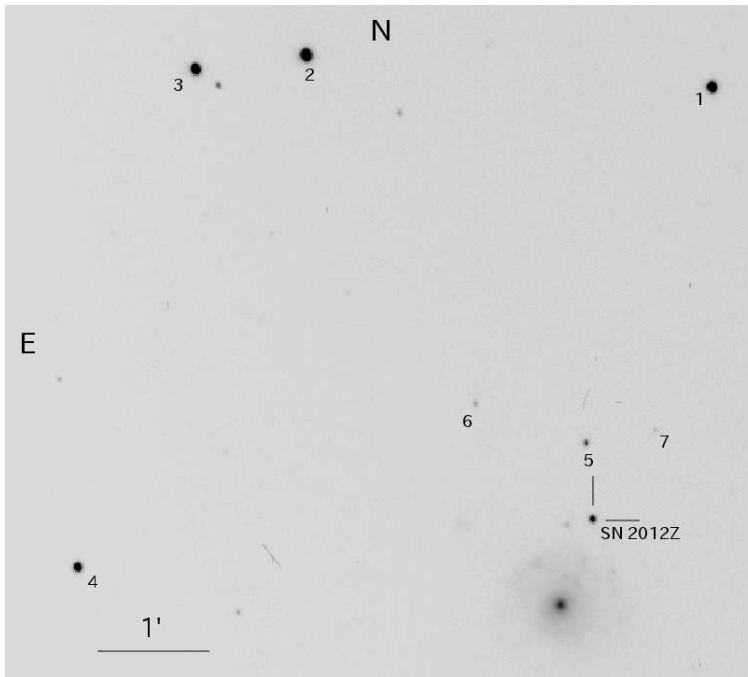
FIG. 1.— The I-band image with SN 2012Z obtained using HOWPol attached to the Kanata telescope on 2012 Feb 12 ($t = +4.1$ d).

3). The wavelength coverage of HOWPol was 4500–9000 Å and the spectral resolution was $R = \lambda/\Delta\lambda \simeq 400$ at 6000 Å; the wavelength coverage of LOSA/F2 was 4200–8000 Å with a spectral resolution of $R \simeq 600$ at 6000 Å. During the data reduction procedure, the wavelengths were calibrated using telluric emission lines acquired in the object frames for the HOWPol data, and using the FeArNe arc lamp frames for the LOSA/F2 data. The fluxes were calibrated using the frames of spectrophotometric standard stars taken on the same night as the object data. We removed the strong telluric absorption features from the object spectra using the spectra of high-temperature standard stars.

2.4. Late phase observations

We performed spectroscopic observations of SN 2012Z using the Faint Object Camera and Spectrograph (FOCAS; Kashikawa et al. 2002) attached to the Cassegrain focus of the 8.2-m Subaru telescope on Oct 23 UT ($t = +261.3$ d). For the shorter wavelength observations, we used a B300 grism. For the longer wavelengths, we used an R300 grism and an O58 order-cut filter. The composite wavelength coverage was 4600–9600 Å. We used the $0''.8$-width slit; the resulting wavelength resolution was $R \simeq 660$ at 6000 Å. During the data reduction procedure, the wavelength was calibrated using the frames of the ThAr arc lamp. We also obtained B, V, R, and I-band imaging observations for the SN and photometric standard stars.

2.5. Photometric calibration

We performed relative photometry using the local reference stars in the field of SN 2012Z (see Figure 1). For the NIR data, we used the magnitudes from the 2MASS catalog for the references stars (Persson et al. 1998). We adopted a square average of the standard deviation of the

SN and the systematic error of the reference star magnitudes for the observational errors. A summary of the results of the NIR photometry is listed in Table 4.

To calibrate the B, V, R, and I-band magnitudes of the reference stars, we used the photometric data of standard stars in the SA95 region (Landolt 1992), which were obtained using HOWPol on a photometric night. We performed relative photometry for the SN commonly using these magnitudes, except for the data of MITSuME at OAO. For the data of MITSuME at OAO, the g', R, and I-band data were calibrated using the SA96 (Landolt 1992) region obtained using the instrument itself. For the U-band data at Pirka, we obtained the magnitude of the references stars using extrapolation with the $U - B$ versus $B - V$ relation of the Landolt standard sequence (Landolt 1992); therefore, the observational error was relatively large. Table 8 lists a summary of the optical photometry data.

Table 5 lists a summary of the obtained magnitudes of the references stars. Note that we reduced the systematic error among the various instruments using a color-term correction in a consistent manner, and included newly performed observations of the standard stars in the M67 (Stetson 1987) and SA98 (Landolt 1992) regions.

3. RESULTS

3.1. Light curves

Figure 2 shows the U, B, g', V, R, I, $z' + Y$, J, H, and K_s-band light curves. Galactic extinctions were corrected for using the color excesses $E(B - V) = 0.036$ mag (Schlafly & Finkbeiner 2011). We assumed negligible host galactic extinction by comparing the color evolutions with those of the same subclass, including the near-infrared photometry.

We found that the B-band maximum magnitude was 14.74 ± 0.01 mag and the date was MJD 55965.8 ± 3.0. The peak date was 1.3 days earlier than that reported

by Stritzinger et al. (2015). This date was assumed as $t = 0$ throughout this paper. We also evaluated the maximum magnitudes and dates in all other bands (see Table 6). As with other SNe Iax, the NIR light curves for SN 2012Z exhibited a single maximum. The maxima for redder bands appeared later. For example, the K_s-band maximum occurred at $t = +16$ d, which was significantly later than that of a typical SN Ia ($t = -3$ d Krisciunas et al. 2003). We calculated the rate of decline of the B-band light curve as $\Delta m_{15}(B) = 1.57 \pm 0.07$ mag, which is slightly larger than that reported by Stritzinger et al. (2015). We also calculated $\Delta m_{15}(\lambda)$ of the V, R, I, J, H, and K_s-band light curves (see Table 6). We found that the rates of decline were smaller in the redder bands, which corresponds to the wider shapes, except for the J-band.

Figure 3 shows the J, H, and K_s-band light curves as well as those of SNe Iax 2005hk ($\Delta m_{15}(B) = 1.7 \pm 0.1$ mag; Phillips et al. 2007), 2008ha ($\Delta m_{15}(B) = 2.17 \pm 0.02$ mag; Foley et al. 2010a) and a normal SN 2001el ($\Delta m_{15}(B) = 1.13 \pm 0.04$ mag; Krisciunas et al. 2003). Our near-infrared light curves exhibited the best time coverage among SNe Iax.

NIR light curves of SN 2012Z and other SNe Iax commonly show a single peak, in contrast to the double peaks observed with normal Type Ia SNe. For the J-band light curves, the overall shape was similar to that of SN 2005hk (at $t = -5 - +60$ d). A small difference was observed in the rise time; i.e., SN 2012Z exhibited a faster rise than did SN 2005hk. SN 2008ha also exhibited a faster decline than SN 2012Z. The magnitude (relative to the maximum) of SN 2008ha was fainter than that of SN 2012Z by $0.5 - 1.0$ mag at $t = +20$ d. Similar trends were also found in the H-band light curves; i.e., SN 2012Z exhibited a faster rise, and SN 2008ha a faster decline. For the K_s band, dense data are not available for other SNe Iax. Two photometric points of SN 2005hk are consistent with those of SN 2012Z.

In summary, the near-infrared light curves were highly similar to those of SN 2005hk among $t = -5 - +60$ d, except during the rise, as determined from the optical bands (Stritzinger et al. 2015).

Figure 4 shows the color indices $V - J$, $V - H$, and $V - K_s$ of SN 2012Z. These data were corrected for Galactic extinctions only. The colors continuously evolved toward the red during our observations. The $V - J$ and $V - H$ evolutions of SN 2012Z were similar to those of SN Iax 2005hk. On the other hand, the color evolutions differed significantly from those of typical SNe Ia. In particular, the $V - J$ color of SNe Iax exhibited monotonic behavior, evolving toward redder colors with time, whereas a typical SN 2001el exhibits non-monotonic behavior, which results from the double-peak light curve in the J band.

Because the near-infrared flux is not attenuated significantly due to dust, the optical to near-infrared wavelengths enable us to estimate the extinction accurately if the intrinsic color is known (Krisciunas et al. 2004). Because the absolute color was consistent with that of the extinction-corrected SN 2005hk ($E(B - V) = 0.09$ mag; Phillips et al. 2007), the extinction of SN 2012Z may be considered negligible. The $V - J$ and $V - H$ colors of SN 2012Z were bluer than those of SN 2008ha, which may result from uncertainties in the color excess (Foley et al.

2013).

The color of the NIR bands was similar to those of SNe Iax, as shown in Figure 5. The $J - H$ and $J - K_s$ color evolutions exhibited a monotonous increase. The $J - K_s$ color evolution was similar to those of SNe 2005hk and 2008ha, despite the sparse data. The $H - K_s$ color was similar to those of SNe 2005hk and 2008ha, although these were sparse. Only the $H - K_s$ color exhibited a similarity between SN 2012Z and normal SNe Ia (see the bottom panel of Figure 5). Such homogeneity in the $H - K_s$ is interesting, whereas all the other colors (V−NIR colors, $J - H$ and $J - K_s$ colors) exhibited a large difference between other SNe Iax and normal SNe Ia.

3.2. *Rise time*

The rise times of SNe Ia have been studied statistically (Hayden et al. 2010; Ganeshalingam et al. 2011; González-Gaitán et al. 2012) and individually (Foley et al. 2012; Silverman et al. 2012; Nugent et al. 2011; Bloom et al. 2012; Yamanaka et al. 2014; Zheng et al. 2013, 2014; Goobar et al. 2014).

SN 2012Z exhibited rapid rises in the B, V, and R bands following its discovery (Cenko et al. 2012b), but was not detected at 3.2 days before discovery (Cenko et al. 2012b). An upper limit of the magnitude was given as $R > 19.0$ mag on Jan 26 ($t \sim -13$ d). We fitted the published data and our data in the B, V, and R-band using a quadratic function, as shown in Figure 6.

We calculated the rise times of SN 2012Z to be 11.8, 12.1, and 12.1 days in the B, V, and R bands, respectively. The average rise time was $t_{rise} = 12.0 \pm 3.0$ days, and the explosion date was MJD 55953.4. The rises of the light curves were well described using single quadratic functions. The smoothly rising curves indicate that there were no strong interactions between the ejecta and companion stars or dense circumstellar materials (CSMs). We discuss possible progenitor systems of SN 2012Z in §4.2.

3.3. *Spectra*

The spectra were compared with those of SN Iax 2005hk (Phillips et al. 2007), as shown in Figure 7. The samples of SN 2005hk were collected from the SUSPECT [21] and WISEREP [22] databases.

At $t = -5$ d, the spectral features were similar to those of SN 2005hk, except for the slightly larger blueshift of all features and the shallower depth. The spectral features at $t = +4$ d also exhibit a slightly larger blueshift than those of SN 2005hk. The C II absorption line was barely observable between $t = +1$ and $t = +12$ d, which may also be a common property with SN 2005hk. The line velocity was ~ 7000 km s^{-1} between $t = +1$ and $+12$ d. Also note that C II was observed only during the post-maximum phase.

The spectrum of SN 2012Z at $t = +261$ d is shown in Figure 8, along with that of SN 2005hk at $t = +377$ d (Sahu et al. 2008). The spectral profiles differed from those of SN 2005hk. Strong emission features were observed around 7200 Å. This feature is blended with the [Ca II] $\lambda\lambda 7291$, 7323 and [Fe II] $\lambda 7155$ emission lines. The
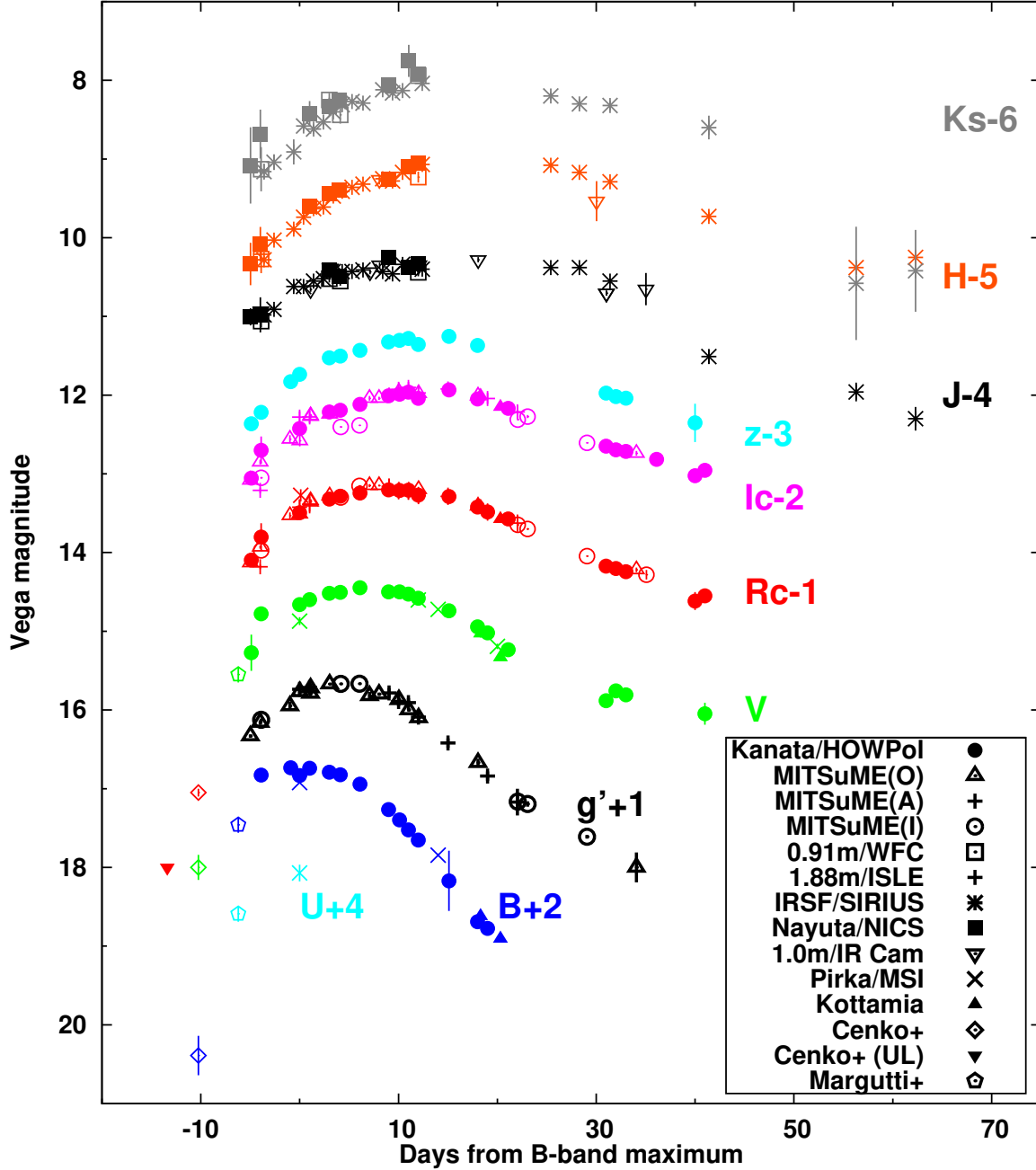
---

[21] http://www.nhn.ou.edu/ suspect/
[22] http://wiserep.weizmann.ac.il/

Fig. 2.— U, B, g', V, R, I, $z'+Y$, J, H, and K_s-band light curves of SN 2012Z. Galactic extinctions were corrected for. The host galactic extinction was negligible. The different colors denote different-band filters, and the shape of the symbols corresponds to the instrument used (see the figure legend). The open-diamond symbols denote the magnitudes reported by Cenko et al. (2012c). The open-pentagon symbols denote the U, B, and V-band magnitudes obtained by $Swfit$/UVOT (Cenko et al. 2012b; Margutti et al. 2012).

emission from the permitted transitions (the Na I D and Ca II IR triplet) were also clearly visible. These features were observed in the spectrum of SN 2005hk; however, the linewidths were significantly broader than those of SN 2005hk. The full-widths at half-maximum (FWHM) values were estimated as 6300, 6200, 5600, and 6300 km s^{-1} for the [Ca II], [Fe II], Na I D, and Ca II IR triplet lines, respectively. The velocities of those lines were approximately 800–1000km s^{-1} for SN 2005hk (Sahu et al. 2008). Such broad emission lines have not been observed in other SNe Iax (Jha et al. 2007; Foley et al. 2013). We

discuss the inner structure of the ejecta in §4.3.

We measured the line velocities of SNe 2012Z and 2005hk. The velocities were estimated from the absorption minima. The recession velocities of the host galaxies were corrected for, according to the values from NED [23]. The line velocities of Si II $\lambda 6355$, Fe III $\lambda 5129$, and Ca II IR triplet of SN 2012Z are shown in Figure 9, and are compared with those of SN 2005hk in Figure 9. The rate of decline of the Si II line velocity was ~ 150 km s^{-1} d^{-1}

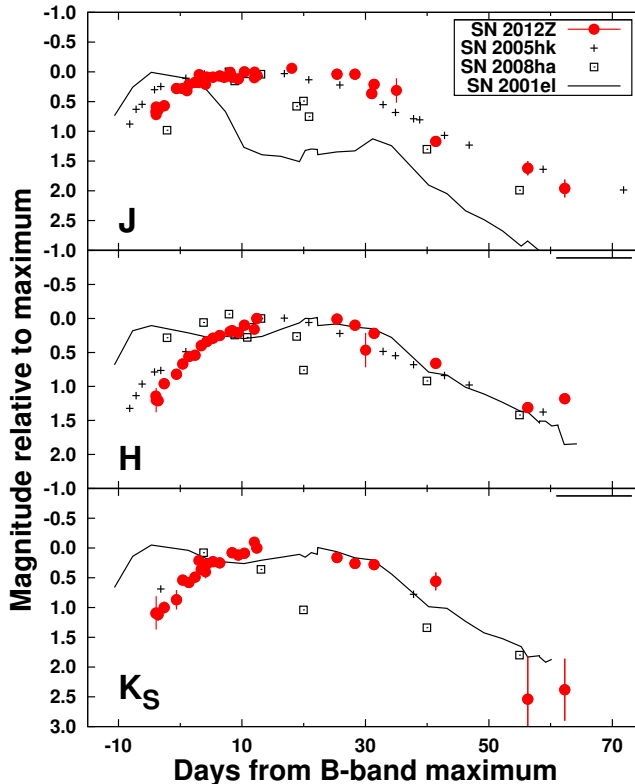[23] NASA/IPAC Extragalactic Database; http://ned.ipac.caltech.edu/

FIG. 3.— J, H, and K_s-band light curves compared with those of SNe 2005hk ($\Delta m_{15}(B)= 1.7\pm0.1$ mag; Phillips et al. (2007)), 2008ha ($\Delta m_{15}(B)= 2.17\pm0.02$ mag; Foley et al. (2010a)) and 2001el ($\Delta m_{15}(B)= 1.13\pm0.04$ mag; Krisciunas et al. (2003)) in the range of $t = -15$ to $+75$ d. The maximum magnitudes were shifted to zero magnitudes for the sake of comparison.

between $t = -5$ and $+10$ d. This is similar to that of SN 2005hk, and as large as that of the high-velocity SNe Ia (Benetti et al. 2005; Yamanaka et al. 2009b). The velocity was 1500 km s^{-1} greater than that of SN 2005hk. After $t = +12$ d, the Si II $\lambda6355$ absorption was strongly blended by other lines, e.g., Fe II (Branch et al. 2004; Sahu et al. 2008). The Fe III line velocity was always 2000 km s^{-1} greater than that of SN 2005hk. We also show the line velocity of the Ca II IR triplet in the bottom panel of Figure 9. The rate of decline appeared to be flat compared with those of Si II and Fe III. A similar trend was also observed for SN 2005hk. Stritzinger et al. (2015) found that the line velocities in Ca II IR triplets and H&K exhibit flat evolutions.

3.4. *Environment*

The environment of the host galaxies of SNe Iax has been investigated based on morphological classifications (Valenti et al. 2009; Foley et al. 2010b) and the strength of the emissions from the HII regions (Lyman et al. 2013). Lyman et al. (2013) reported that the distribution of Hα intensities of SN locations for SNe Iax is similar to that of core collapse Type IIP SNe. The host galaxies of most SNe Iax are spiral galaxies, and include some star-forming regions (see also Foley et al. 2010a; Valenti et al. 2009) (except for that of SN 2008ge (Foley et al. 2010b)). The samples include SN 2012Z. However, measurements of the metallicity of the explosion locations are rare for SNe Iax.

The FOCAS spectrum at $t = +261$ d exhibited weak emission lines of Hα, [N II]$\lambda6583$, Hβ, and O III$\lambda5007$. Using the O3N2 metallicity indicator (i.e., the ratio of [N II]/Hα to [O III$\lambda5007$/Hβ) Pettini & Pagel (2004)), we estimate the metallicity as $12+\log(O)< 8.51 \pm 0.31$. This is consistent with those of the previous two objects. These observations indicate that the environment of SN 2012Z might be similar to those of SNe 2008ha and 2010ae (Foley et al. 2010a; Stritzinger et al. 2014).

3.5. *Quasi-bolometric light curves*

To determine the kinetic energy and ejecta mass of SN 2012Z, we compare the quasi-bolometric light curve with an analytic model. First, we constructed quasi-bolometric light curves for SNe 2012Z and 2001el. The B, V, R, I, J, H, and K_s-band fluxes were integrated using each filter passband function (Bessell 1990; Bessell et al. 1998). The ratio of the fluxes of the NIR (J, H, and K_s bands) to the integrated fluxes (B, V, R, I, J, H, and K_s bands) at peak luminosity was estimated to be ~ 0.20 for SN 2012Z, which is larger than that of a normal SN Ia (~0.1; Wang et al. 2009). We assume that the B, V, R, I, J, H, and K_s-band fluxes contribute 80% of the total bolometric luminosity (Stritzinger et al. 2006). The rise time was $t_{rise} = 12.0$ days. The ^{56}Ni mass was estimated to be $\sim 0.18 M_\odot$, which is considerably smaller than the average mass of SNe Ia , although the uncertainty is relatively large due to the uncertainty in the rise time.

The ratio of the evolution of the NIR to the integrated flux exhibited a monotonic increase from $+8$ to $+25$ days
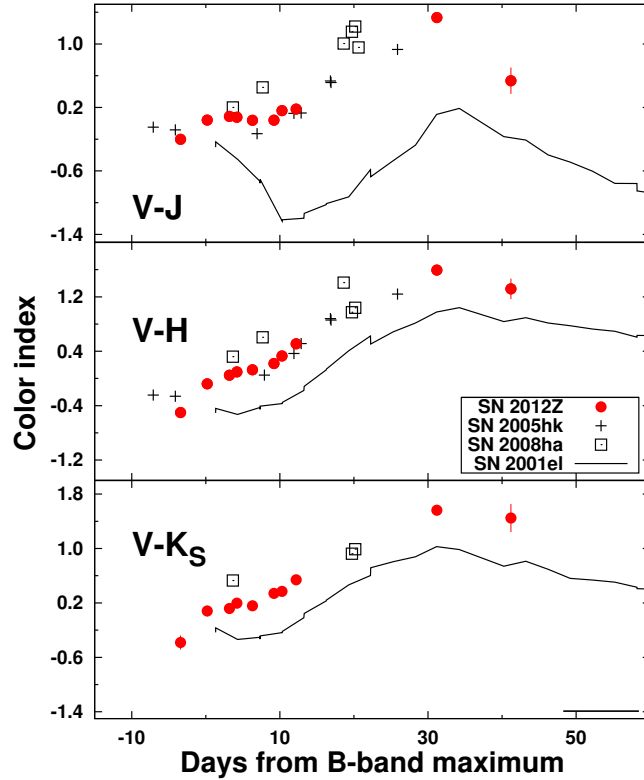
Fig. 4.— $V - J$, $V - H$, and $V - K_s$ color evolutions plotted together with those of SNe 2005hk, 2008ha, and 2001el. Galactic and host galactic extinctions are corrected for.

since the explosion date. This differs significantly in comparison with typical SNe Ia (Wang et al. 2009), but is consistent with the $V - NIR$ color evolutions (see §3.1).

The quasi-bolometric light curve was compared with an analytical model derived using Maeda et al. (2003)

$$L(t) = M_{56\mathrm{Ni}}((S_{56\mathrm{Ni}} + S_{56\mathrm{Co}})(1 - e^{-\tau}) + S_{56\mathrm{Co}} \cdot f_p), \quad (1)$$

where $M_{56\mathrm{Ni}}$ is the mass of the ejected ^{56}Ni and f_p is the positron fraction. The energy release rates ($S_{56\mathrm{Ni}}$ and $S_{56\mathrm{Co}}$) are expressed as

$$S_{56\mathrm{Ni}} = (3.90 \times 10^{10}) e^{-t/t_{56\mathrm{Ni}}} \mathrm{erg \ s^{-1} \ g^{-1}} \quad (2)$$

and

$$S_{56\mathrm{Co}} = (7.01 \times 10^9)(e^{-t/t_{56\mathrm{Co}}} - e^{-t/t_{56\mathrm{Ni}}}) \ \mathrm{erg \ s^{-1} \ g^{-1}}. \quad (3)$$

The decay timescales are $t_{56\mathrm{Ni}} = 8.8$ and $t_{56\mathrm{Co}} = 113.5$ days, respectively. τ is given by

$$\tau = 1000(Mej^2/M_\odot)(E_k^{-1}/10^{51}\mathrm{erg \ s^{-1}})(t/day)^{-2}, \quad (4)$$

where M_{ej} is the mass and E_k is the kinetic energy of the ejected material.

The ratio of the ejected mass to the kinetic energy is given by $(M_{ej}/M_\odot)^2 \cdot (E_k/10^{51} \ \mathrm{erg \ s^{-1}})^{-1} = 2.45$ by comparing the analytical light curve with our observed light curve. This degeneracy can be resolved by adding photospheric velocity data. As a proxy of the photospheric velocity, we used the Si II line velocity, which was $\sim$7000km s^{-1} (see §3.3). Note that the Si II velocity was slightly larger than the photospheric velocity (Fisher et al. 1997). This should result in a kinetic energy increase or mass decrease. We calculated the ejected

mass to be $M_{ej} \sim 1.15$ M$_\odot$ and the kinetic energy to be $E_K \sim 0.5 \times 10^{51}$ erg s^{-1} , while Stritzinger et al. (2015) estimated the ejected mass as $1.4 - 1.9$ M$_\odot$ using their calculations. We emphasize that our analysis contains some uncertainties. For example, the same opacity was assumed as that of a normal SN Ia. The effective opacity may have a strong dependence on the temperatures (e.g., Hoeflich et al. 1992), i.e., more luminous events can have higher opacities. It is, in fact, one of the promising explanation for the width-luminosity relation of normal SNe Ia (Hoeflich et al. 1996; Nugent et al. 1997; Maeda et al. 2003; Kasen & Woosley 2007; Baron et al. 2012). If this trend is also true for SNe Iax, the effective opacity in the ejecta of SN 2012Z may be lower than in the ejecta of normal SNe Ia. Therefore, our estimated mass could be just a lower limit. Furthermore, a quantitative uncertainty exists in the density profile. Thus, detailed radiative transfer calculations are desirable. In §4.3, we use only E_k and M_{ej} to estimate the upper limit of the shock luminosity. The late-phase luminosity could not be explained completely using our analytical light curves. The diversity of the decline rates may be significant among SNe Iax during the late phase (Stritzinger et al. 2015).

4. DISCUSSION

4.1. Comparison of the NIR properties with other SNe Iax

We found no secondary maxima in the NIR light curves, and the form of the color evolutions were similar to those of SNe 2005hk and 2008ha, as discussed in §3.1. Due to the small number of samples of NIR light
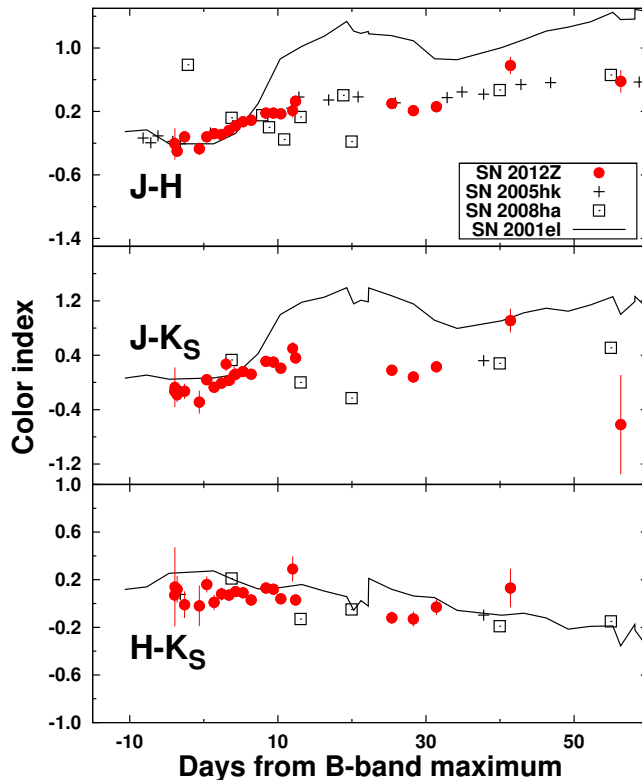
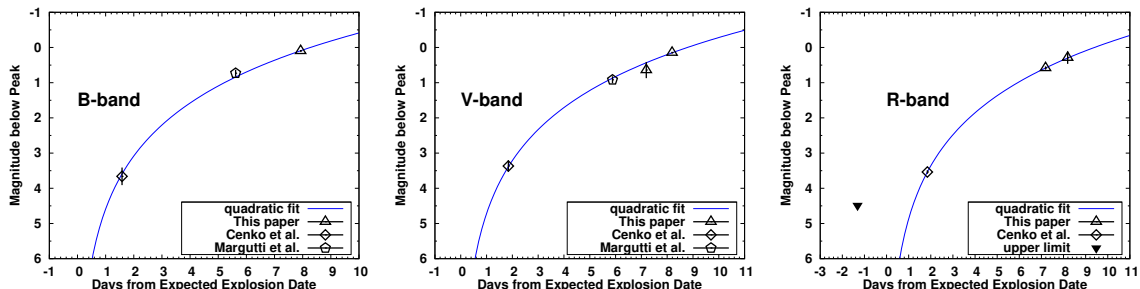Fig. 5.— Same as Figure 4, but for NIR-NIR color evolutions.

Fig. 6.— B, V, and R-band rise curves of SN 2012Z with quadratic fits (shown by blue doted curves). These data include the b and v magnitudes obtained using the $Swift/UVOT$ telescope (Margutti et al. 2012), and the immediately observed B, V, and R-band data obtained using LOSS (Cenko et al. 2012c) and HOWPol. The filled triangle symbols in the right panel denote the upper-limit magnitudes reported by Cenko et al. (2012b). The maximum magnitudes were shifted to zero.

curves, the NIR absolute magnitudes have not yet been well characterized for SNe Iax. It remains ambiguous whether the rates of decline correlate with the absolute magnitudes in the NIR bands. Such a correlation would mean that SN Iax explosions may have a single origin (Foley et al. 2013). Here, we focus on the relationship between the NIR absolute magnitudes and rates of decline of the light curves.

The absolute magnitudes and the rates of decline of SN 2012Z in the J, H, and K_s bands were compared with those of other SNe Ia (Krisciunas et al. 2004) and SNe Iax 2005hk (Phillips et al. 2007), 2008ha (Foley et al. 2010a), and 2010ae (Stritzinger et al. 2014), as shown in Figure 10. In the J and H bands, the locations ($M_J \sim -18.1$ mag, $M_H \sim -18.3$ mag, and $\Delta m_{15}(B) = 1.6 \pm 0.1$ mag)

of SN 2012Z were close to those of SN 2005hk. In contrast, the absolute magnitudes of SNe 2008ha and 2010ae were significantly fainter than those of SN 2012Z. The K_s-band absolute magnitude ($M_{K_s} \sim -18.3$ mag) of SN 2012Z was similar to that of SNe Ia. Although the number of samples was limited, we found a correlation between the rates of decline of the light curves and the absolute magnitudes. However, larger samples are required to conclude whether the origin of SNe Iax is homogeneous.

4.2. Comparison of rise times

We precisely calculated the rise time of a SN Iax for the first time (see §3.2). Phillips et al. (2007) reported a rise time of 15.0 ± 0.1 days for SN 2005hk using a quadratic
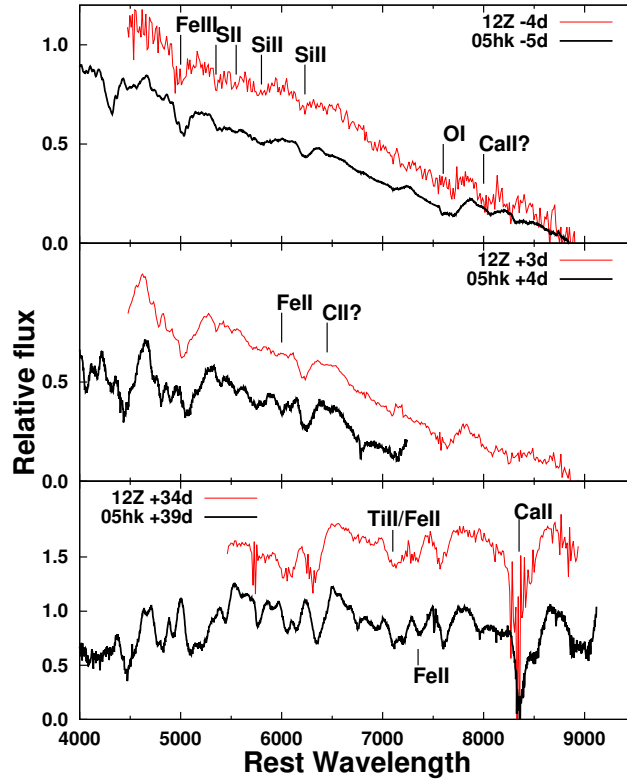
FIG. 7.— (Top panel) Spectrum of SN 2012Z at $t = -4$ d compared with that of Type Iax SN 2005hk (Phillips et al. 2007) at $t = -5$ d. The wavelength was calibrated to the rest frame of each host galaxy. The spectrum exhibited Si II$\lambda 6355$, Si II$\lambda 5972$ and S II W-shape features as well as Fe III λ 5267 absorption lines. The Ca II IR triplet and O I $\lambda 7774$ were also detected. (Middle panel) Same as the top panel, but at $t = +3$ d. Possible C II $\lambda 6580$ absorption lines were observed. (Bottom panel) Same as the top panel, but at $t = 34$d. Many Fe II absorption lines were clearly visible.
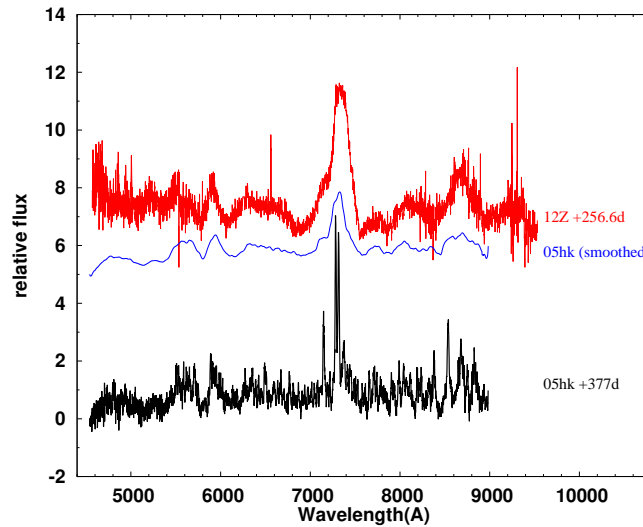
FIG. 8.— Nebular spectrum of SN 2012Z at $t = 256.6$ d (red curve) and the spectrum of SN 2005hk (Sahu et al. 2008) at $t = 377$ d (black curve). The blue curve denotes the artificially broadened spectrum of SN 2005hk.

Yamanaka et al.
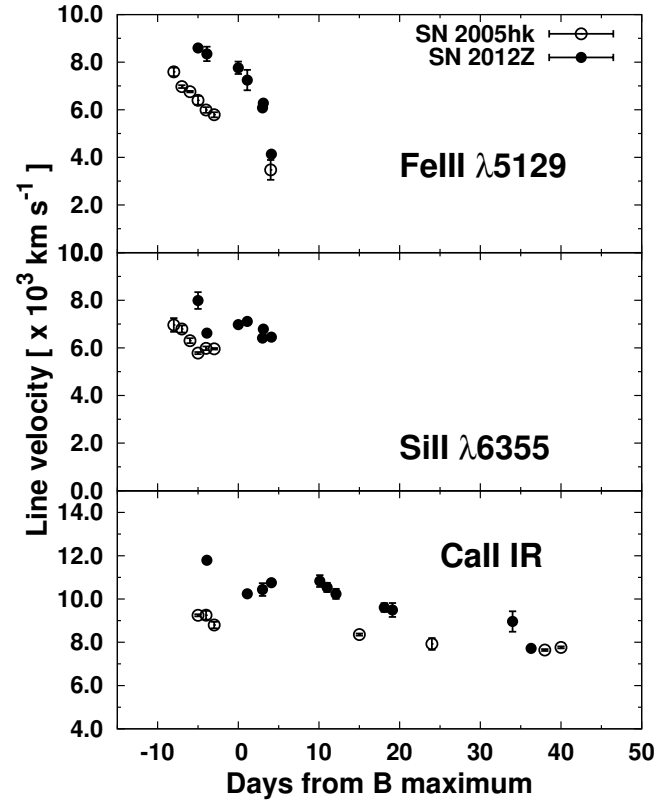
FIG. 9.— (Top panel) Fe IIIλ5129 line velocity evolution of SN 2012Z (filled circles). This is compared with that of SN 2005hk (open circles). The horizontal axis is days from the B-band maximum. (Middle panel) Same as the top panel, but the Si IIIλ6355 lines are shown. (Bottom panel) Same as the top panel, but the Ca II IR triplet lines are shown.
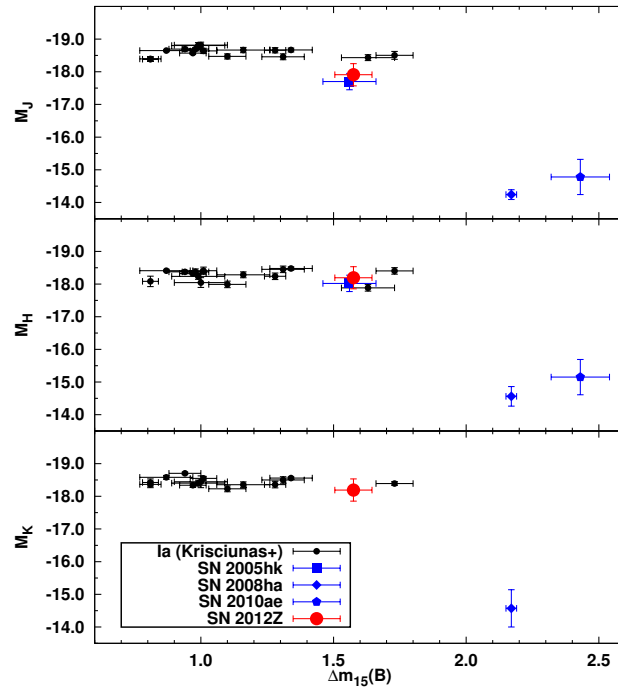
FIG. 10.— J, H, and K_s-band absolute magnitudes plotted as functions of the rate of decline $\Delta m_{15}(B)$ (red symbols). Also shown are those of other typical SNe Ia (Krisciunas et al. 2004) (blue symbols). The absolute magnitudes were calibrated using distance moduli to the host galaxies.

fit to the first two photometric points. We used the same method to calculate the rise time of SN 2012Z.

Figure 11 shows the rise time and $\Delta m_{15}(B)$ of these two SNe Iax and other SNe Ia. Yamanaka et al. (2014) measured the rise times of SNe Ia directly. The rise times calculated using template-fitting methods are also plotted. The rise times for SNe Ia were $17-19$ days, and the rise time of SN 2012Z was 12.0 ± 3.0 days, which is significantly faster than any other SNe Ia, including those calculated using template-fitting extrapolation methods (Ganeshalingam et al. 2011).

The quadratic fit of the light curves to SNe Iax has been problematic, because of a paucity of data during the rising phase. The rise times of individual SNe Iax have been discussed using various methods. Foley et al. (2010a) calculated the rise time of SN 2008ha as ∼10 days using a scaling method based on the light curves of SN 2005hk. Narayan et al. (2011) also used a scaling method to calculate the rise time of SN 2009ku, and reported the rise time as ∼ 18.2 ± 3.0 days. McClelland et al. (2010) inferred the rise time of SN 2007qd as 10 ± 2 days using the previous upper limit magnitudes prior to its discovery. Foley et al. (2010b) reported that the rise time of SN 2008ge should be between 9 and 27 days based on its spectral evolution.

These indicate that the rise times of SNe Ia exhibit a variety, which may reflect the diversity of the ^{56}Ni distributions in the outer layer (Piro 2012; Piro & Nakar 2013, 2014). The short rise time of SN 2012Z suggests that the mixing of the ejecta produces the extended ^{56}Ni distributions (Piro & Nakar 2014). Furthermore, the NIR light curves exhibit no secondary maxima (see §3.1). This indicates that ejecta mixing likely occurred (Blinnikov et al. 2006; Kasen 2006). The homogeniety of the NIR light curves implies that mixing is a common property shared by SNe Iax. Thus, the theoretical models must simultaneously describe the homogeneous NIR light curves and the diverse rise times.

It is noted that the opacity can also affect the rise time. Lower effective opacity results in the faster rise of the light curves. As mentioned in §3.5. a lower luminosity may give a lower opacity of the ejecta, and the effective opacity for SN 2012Z may be lower than that in normal SNe Ia (Stritzinger et al. 2015).

The variety of rise times may result in an over- or under- estimate of the ^{56}Ni masses. To determine the rise time with improved accuracy, a high-cadence survey of the SN discoveries at nearby galaxies is required.

4.3. Progenitor systems

In this section we discuss the nature of the possible companion star. The rising curves were satisfactorily fitted using a quadratic function (see §3.3). However, ejecta-companion interaction models predict bright shock luminosity during the rising phase, especially for the bluer bands (Kasen 2010), yet such signatures were not observed in our measurements. The existence of a giant companion is, therefore, not supported; however, we note that the strength of this signal is expected to be dependent on the viewing direction.

The environments around SNe Iax are similar to those of core collapse SNe IIP (Lyman et al. 2013). For SN 2012Z, the age of the progenitor has been estimated to be $30-50$ Myr (Lyman et al. 2013). Recently binary evolution studies (Meng & Podsiadlowski 2014; Wang et al. 2014; Liu et al. 2015) have shown that the delay times for explosions are as less than 100 Myr for WD + He binary systems. We found that the H II region existed at the projected distance of ∼ 90pc to SN 2012Z, indicating a young population as also inferred by the low metallicity. This is consistent with the compact blue source in the pre-explosion image (McCully et al. 2014).

The upper limit of the progenitor radius was calculated following Yamanaka et al. (2014). Shock breakout is expected when the early phase when the ejecta bursts through a progenitor, and the deposited energy is released during the early phase (Rabinak & Waxman 2011; Piro & Nakar 2013). This emission becomes more luminous when the progenitor has a larger radius. In the extreme case, the upper limit of luminosity for SN 2011fe was given on just 0.2 days after the explosion (Bloom et al. 2012). Its progenitor radius has been reported as limited to at most $0.02R_{\odot}$ (Bloom et al. 2012). For SN 2012Z, the luminosity was obtained at 2.0 days following the explosion (Cenko et al. 2012b). To eliminate uncertainties in the models, we scaled the upper limit of the luminosity of SN 2011fe (Bloom et al. 2012) to that of SN 2012Z (see Yamanaka et al. 2014, for details). We assumed the kinetic energy was $E_K = 0.5 \times 10^{51} erg\ s^{-1}$ and the mass of the ejecta was $M_{ej} = 1.15 M_{\odot}$ (see §3.5 and Figure 12). Note that the normalized density profile of the progenitor as well as the opacity were assumed to be the same as those of SN 2011fe. We obtained an upper limit for the radius of SN 2012Z as ∼2.0 $R_{\odot}$. This ruled out an extended progenitor star like a red giant (Rabinak & Waxman 2011). Scenarios with WD progenitors (both single degenerate and double degenerate) were therefore supperted.

4.4. Ejecta Structure

The emission lines during the late epoch were 6–8 times broader than those of SN 2005hk, whereas the early-phase properties were similar. The artificially broadened line profiles of SN 2005hk matched with those of SN 2012Z, as shown in Figure 8 (Sahu et al. 2008; Stritzinger et al. 2015). This suggests that the temperature and density of inner ejecta of SN 2012Z were similar to those of SN 2005hk; however, the velocity and thus spatial extent of the emission region were larger for SN 2012Z. In contrast to the large difference in the late-phase spectra, the early-phase spectra and the light curves of SN 2005hk and SN 2012Z were similar. Thus, we speculate that the ejecta of SN 2005hk and SN 2012Z had a similar structure in the outer layer, whereas the ejecta of SN 2012Z had a more extended inner core.

4.5. Explosion models

Here, we compare the observed properties of SN 2012Z with the characteristic features predicted by the following explosion models: pure deflagration, failed deflagration, double detonation, pulsating delayed detonation, and core collapse. Table 7 lists a summary of these comparisons.

A pure deflagration model (Gamezo et al. 2003) has been suggested for SNe Iax (Phillips et al. 2007). The light curves and spectral evolutions have been synthesized via radiative transfer calculations (Blinnikov et al.
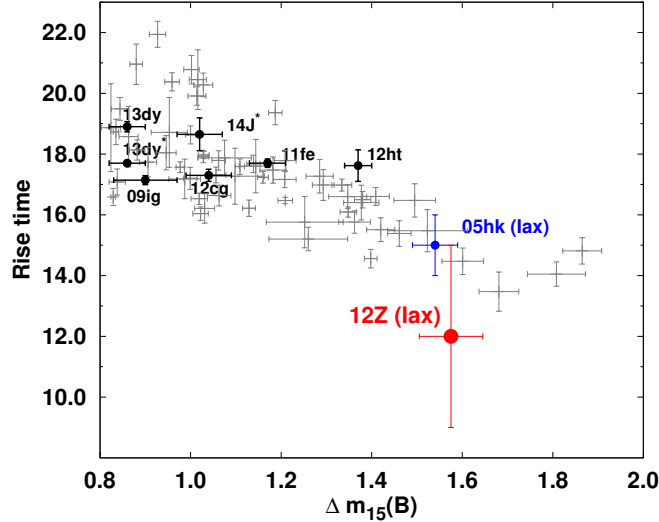
FIG. 11.— Rate of decline $\Delta m_{15}(B)$ and rise time of SN 2012Z, as well as those of SN 2005hk (Phillips et al. 2007), 2009ig (Foley et al. 2012; Marion et al. 2013), 2011fe (Nugent et al. 2011; Pereira et al. 2013), 2012cg (Silverman et al. 2012; Munari et al. 2013), 2012ht (Yamanaka et al. 2014), 2013dy (Zheng et al. 2013), and 2014J (Zheng et al. 2014). The rise time of SN 2013dy was found to be 17.7 days based on a broken power-law fitting, whereas it was ~ 18.9 days using a quadratic fit (Zheng et al. 2013). The gray cross symbols show template-fitting data from Ganeshalingam et al. (2011).
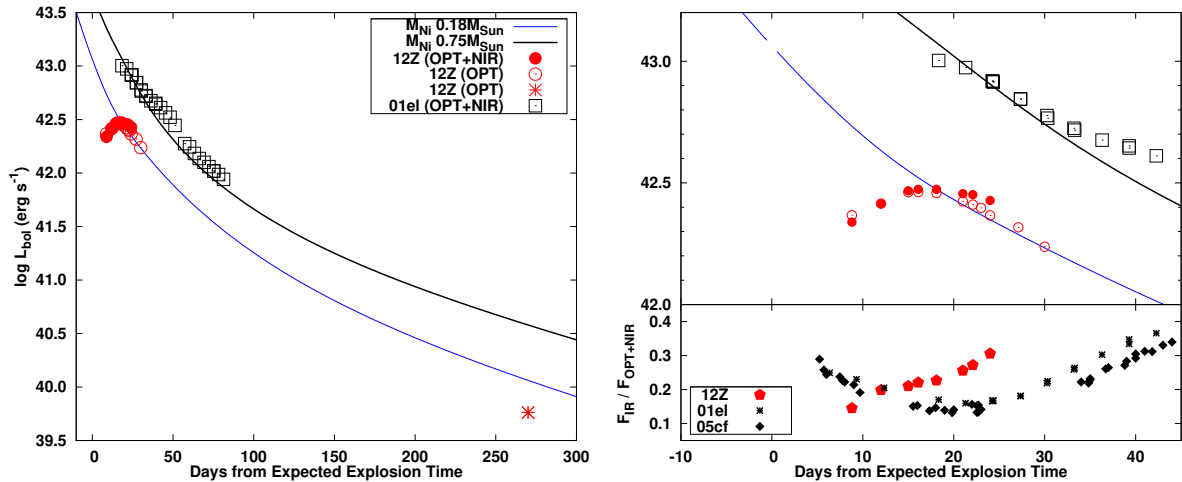

FIG. 12.— (Left panel) Quasi-bolometric light curves of SN 2012Z and normal SN Ia 2001el, both at the estimated explosion date and 300 days later. The open circles show the quasi-bolometric light curve integrated using $BVRI$-band data, and the filled circles show the light curves integrated using $BVRIJHK_s$-band data. The late-phase luminosity at $t = 280$ was the only $BVRI$-band integration point. The plotted $BVRI$-band curves were corrected for by multiplying the original flux by a factor of 1.25. For SN 2001el, the $BVRIJHK_s$-band data were integrated, as shown by the black open-square symbols. The blue curve shows the analytical result for $M(^{56}\mathrm{Ni}) = 0.18M_\odot$, $M_\mathrm{ej} = 1.15M_\odot$, and $E_\mathrm{K} = 0.5$ erg s^{-1}. The black curve shows that with $M(^{56}\mathrm{Ni}) = 0.75M_\odot$, $M_\mathrm{ej} = 1.4M_\odot$ and $E_\mathrm{K} = 1.4 \times 10^{51}$ erg s^{-1}. (Right top panel) Same as the left panel, showing a close-up quasi-bolometric light curve of the expected explosion date and 50 days later. (Right bottom panel) Evolution of the ratio of the integrated JHK_s-band to the $BVRIJHK_s$-band flux, including data for SNe Ia 2001el and 2005cf (Wang et al. 2009).

2006; Röpke et al. 2007; Long et al. 2014) based on three-dimensional deflagrations models. The small amount of ejected ^{56}Ni and the slow expansion are consistent with those of SNe Iax. There was also no secondary maximum in the theoretical NIR light curves, which is interpreted as a mixing within the ejecta (Kasen 2006); this is consistent with the observations. However, the rise time predicted by the model was significantly longer than our calculated rise time (Blinnikov et al. 2006). The luminosity of SNe 2008ha and 2010ae may be too faint to compare to the predictions from such explosion models.

A failed deflagration model has also been suggested for SNe Iax (Jordan et al. 2012; Kromer et al. 2013; Fink et al. 2014). Fink et al. (2014) indicated that part of the ejecta is bound due to the small input energy. The mass of the compact remnant has been predicted to be $\sim 1.0\ M_\odot$. The small ejected mass is qualitatively consistent with our estimate of the ejecta mass of SN 2012Z,

which is potentially smaller than the Chandrasekhar limiting mass. The predicted mass in this particular model is smaller than our estimate, but we note there are uncertainties both in models and observationally derived ejecta mass. Fink et al. (2014) constructed synthetic spectra using their models; the blue continuum, highly excited features, and low velocities of the elements in the spectra were similar to the spectra of SNe 2005hk and 2012Z. The form of the light curve and the absolute luminosities were also well reproduced (Fink et al. 2014). Kromer et al. (2013) reported that the rise time in their models was ∼11 days, which is consistent with that of SN 2012Z. A compact remnant may also be consistent with the red source of SN 2008ha detected 1500 days after the explosion using HST archival images (Foley et al. 2014).

Detection of possible He donors in the pre-explosion image (McCully et al. 2014) may indicate a double-detonation scenario, triggered by He accretion due to a companion star (Nomoto 1982; Woosley & Weaver 1994). Although our spectra do not exhibit any He I emission lines, a few SNe Iax do (Foley et al. 2013). However, the expected rise time, expansion velocity, and absolute luminosity are quite different from our data (Sim et al. 2013). This suggests that the detected pre-SN point source was not a He donor, or challenges a theoretical model that an He accretion results in the double-detonation.

Stritzinger et al. (2015) compared their observations of SN 2012Z with the pulsational delayed detonation (PDD) model, in which a detonation is triggered following a failed deflagration (Bravo & García-Senz 2006). Stritzinger et al. (2015) reported that the decline of the line velocity in Ca II H&K and the flat-topped line profile of [Fe II] $\lambda 1.64$ μm during the late phase supports the PDD model. The rapid rise and the low luminosity can also be reproduced by the PDD model (Baron et al. 2012). The higher luminosity should follow the later maximum in the NIR bands. Such effect may explain the single peak in the I, J, H, and K_s bands (Hoeflich et al. 1995). The PDD may be another attractive scenarios in these aspects.

Finally, we compare our observations with the behavior predicted by a core collapse scenario. Moriya et al. (2010) reported that the wide range of absolute luminosities observed in SNe Iax could be reproduced by this model. The rapid rise may also be explained; however, the quasi-bolometric light curves and the Si II velocity favor $M_{ej} = 1.15 M_\odot$ and $E_k = 0.5 \times 10^{51}$ erg s^{-1}, which cannot be reproduced by a core collapse scenario.

Table 7 lists a summary of these comparisons. The failed deflagration model is the most favored scenario to describe the observed properties of SN 2012Z, as well as other SNe Iax. However, as discussed in §4.2, SNe Iax exhibit varied rise times; it follows that the ^{56}Ni distributions in the outer part of the ejecta may also be diverse among SNe Iax. More comprehensive explosion models are required to describe both the diversity and homogeneity.

5. CONCLUSIONS

We have carried out optical and near-infrared observations of the SN Iax 2012Z from immediately after the explosion to $t = +261$ d. We have described long-duration observations of the J, H, and K_s-band light curves of a SN Iax for the first time. Our findings are summarized as follows.

- There were no secondary maxima in the J, H, and K_s bands. The NIR light curves and color evolutions of SN 2012Z were very similar to those of other SNe Iax.

- The J and H-band absolute magnitudes were $M_J \sim -18.1$ mag and $M_H \sim -18.3$ mag, and the rate of decline of the B-band light curve was $\Delta m_{15}(B) = 1.6 \pm 0.1$ mag. These are very similar to those of the bright SN Iax 2005hk; however, SN 2012Z was more luminous than the faint SNe Iax 2008ha and 2010ae.

- The rise time was calculated to be 12.0 ± 3.0 days, which is significantly shorter than 15.0 ± 0.1 days for SN 2005hk. The rise times of SNe Iax may exhibit significant diversity.

- The explosion site was characterized by low metallicity and a moderate star-forming environment; this is consistent with the binary evolution models of an He star. However, the popular explosion scenario for such a system (i.e., double detonation) is not compatible to the observed SN properties.

The rapid rise indicates that ^{56}Ni was present in the outer layer. The single peak of the NIR light curves also suggests mixing of iron-peak elements throughout the ejecta. These properties may be also explained by the opacity effect. The rise indicates that the progenitor was more compact than a red giant.

Comparing our observations with the theoretical models, the most probable scenario appears to be the failed deflagration model, although PDD model (Stritzinger et al. 2015) is not excluded. The large diversity of the rise times observed in SNe Iax requires a more comprehensive theoretical analysis. The observations indicate that they may originate from a homogeneous population. There appears to be a diverse range of rise times, however, and bright SNe Iax samples are required to further investigate this. A high-cadence survey of nearby galaxies is therefore encouraged.

REFERENCES

Aldering, G., Antilogus, P., Bailey, S., et al. 2006, ApJ, 650, 510

Altavilla, G., Fiorentino, G., Marconi, M., et al. 2004, MNRAS, 349, 1344

Baron, E., Höflich, P., Krisciunas, K., et al. 2012, ApJ, 753, 105

Benetti, S., Cappellaro, E., Mazzali, P. A., et al. 2005, ApJ, 623, 1011

Bessell, M. S. 1990, PASP, 102, 1181

Bessell, M. S., Castelli, F., & Plez, B. 1998, A&A, 333, 231

Blinnikov, S. I., Röpke, F. K., Sorokina, E. I., et al. 2006, A&A, 453, 229

Bloom, J. S., Kasen, D., Shen, K. J., et al. 2012, ApJ, 744, L17

Branch, D., Baron, E., Thomas, R. C., et al. 2004, PASP, 116, 903

Bravo, E., & García-Senz, D. 2006, ApJ, 642, L157

Cenko, S. B., Cohen, D. P., Filippenko, A. V., Silverman, J. M., & Ganeshalingam, M. 2012a, The Astronomer's Telegram, 3901, 1

Cenko, S. B., Li, W., & Filippenko, A. V. 2012b, The Astronomer's Telegram, 3900, 1

Cenko, S. B., Li, W., Filippenko, A. V., et al. 2012c, Central Bureau Electronic Telegrams, 3014, 1

Conley, A., Sullivan, M., Hsiao, E. Y., et al. 2008, ApJ, 681, 482

Filippenko, A. V., Li, W. D., Treffers, R. R., & Modjaz, M. 2001, in Astronomical Society of the Pacific Conference Series, Vol. 246, IAU Colloq. 183: Small Telescope Astronomy on Global Scales, ed. B. Paczynski, W.-P. Chen, & C. Lemme, 121

Fink, M., Kromer, M., Seitenzahl, I. R., et al. 2014, MNRAS, 438, 1762

Fisher, A., Branch, D., Nugent, P., & Baron, E. 1997, ApJ, 481, L89

Folatelli, G., Phillips, M. M., Burns, C. R., et al. 2010, AJ, 139, 120

Foley, R. J., Brown, P. J., Rest, A., et al. 2010a, ApJ, 708, L61

Foley, R. J., McCully, C., Jha, S. W., et al. 2014, ApJ, 792, 29

Foley, R. J., Rest, A., Stritzinger, M., et al. 2010b, AJ, 140, 1321

Foley, R. J., Challis, P. J., Filippenko, A. V., et al. 2012, ApJ, 744, 38

Foley, R. J., Challis, P. J., Chornock, R., et al. 2013, ApJ, 767, 57

Gamezo, V. N., Khokhlov, A. M., Oran, E. S., Chtchelkanova, A. Y., & Rosenberg, R. O. 2003, Science, 299, 77

Ganeshalingam, M., Li, W., & Filippenko, A. V. 2011, MNRAS, 416, 2607

González-Gaitán, S., Conley, A., Bianco, F. B., et al. 2012, ApJ, 745, 44

Goobar, A., Johansson, J., Amanullah, R., et al. 2014, ApJ, 784, L12

Hamuy, M., Phillips, M. M., Suntzeff, N. B., et al. 2003, Nature, 424, 651

Hayden, B. T., Garnavich, P. M., Kasen, D., et al. 2010, ApJ, 722, 1691

Hicken, M., Garnavich, P. M., Prieto, J. L., et al. 2007, ApJ, 669, L17

Hoeflich, P., Khokhlov, A., & Mueller, E. 1992, A&A, 259, 549

Hoeflich, P., Khokhlov, A., Wheeler, J. C., et al. 1996, ApJ, 472, L81

Hoeflich, P., Khokhlov, A. M., & Wheeler, J. C. 1995, ApJ, 444, 831

Howell, D. A., Sullivan, M., Nugent, P. E., et al. 2006, Nature, 443, 308

Iijima, T., & Nakanishi, H. 2008, A&A, 482, 865

Jha, S., Riess, A. G., & Kirshner, R. P. 2007, ApJ, 659, 122

Jordan, IV, G. C., Perets, H. B., Fisher, R. T., & van Rossum, D. R. 2012, ApJ, 761, L23

Kamath, U. S., & Anupama, G. C. 2002, Bulletin of the Astronomical Society of India, 30, 679

Kasen, D. 2006, ApJ, 649, 939

—. 2010, ApJ, 708, 1025

Kasen, D., & Woosley, S. E. 2007, ApJ, 656, 661

Kashikawa, N., Aoki, K., Asai, R., et al. 2002, PASJ, 54, 819

Kawabata, K. S., Nagae, O., Chiyonobu, S., et al. 2008, in Society of Photo-Optical Instrumentation Engineers (SPIE) Conference Series, Vol. 7014, Society of Photo-Optical Instrumentation Engineers (SPIE) Conference Series

Kotani, T., Kawai, N., Yanagisawa, K., et al. 2005, Nuovo Cimento C Geophysics Space Physics C, 28, 755

Krisciunas, K., Suntzeff, N. B., Candia, P., et al. 2003, AJ, 125, 166

Krisciunas, K., Suntzeff, N. B., Phillips, M. M., et al. 2004, AJ, 128, 3034

Kromer, M., Fink, M., Stanishev, V., et al. 2013, MNRAS, 429, 2287

Landolt, A. U. 1992, AJ, 104, 340

Li, W., Filippenko, A. V., Chornock, R., et al. 2003, PASP, 115, 453

Liu, Z.-W., Moriya, T. J., Stancliffe, R. J., & Wang, B. 2015, A&A, 574, A12

Long, M., Jordan, IV, G. C., van Rossum, D. R., et al. 2014, ApJ, 789, 103

Lyman, J. D., James, P. A., Perets, H. B., et al. 2013, MNRAS, 434, 527

Maeda, K., Mazzali, P. A., Deng, J., et al. 2003, ApJ, 593, 931

Margutti, R., Milisavljevic, D., & Soderberg, A. 2012, The Astronomer's Telegram, 3909, 1

Marion, G. H., Vinko, J., Wheeler, J. C., et al. 2013, ApJ, 777, 40

McClelland, C. M., Garnavich, P. M., Galbany, L., et al. 2010, ApJ, 720, 704

McCully, C., Jha, S. W., Foley, R. J., et al. 2014, ApJ, 786, 134

Meng, X., & Podsiadlowski, P. 2014, ApJ, 789, L45

Meyer, S., Emig, K., Kaleida, C., & Mamajek, E. E. 2012, Central Bureau Electronic Telegrams, 3014, 2

Moriya, T., Tominaga, N., Tanaka, M., et al. 2010, ApJ, 719, 1445

Munari, U., Henden, A., Belligoli, R., et al. 2013, New A., 20, 30

Nagayama, T., Nagashima, C., Nakajima, Y., et al. 2003, in Society of Photo-Optical Instrumentation Engineers (SPIE) Conference Series, Vol. 4841, Instrument Design and Performance for Optical/Infrared Ground-based Telescopes, ed. M. Iye & A. F. M. Moorwood, 459–464

Narayan, G., Foley, R. J., Berger, E., et al. 2011, ApJ, 731, L11

Nomoto, K. 1982, ApJ, 257, 780

Nomoto, K., Thielemann, F., & Yokoi, K. 1984, ApJ, 286, 644

Nugent, P., Baron, E., Branch, D., Fisher, A., & Hauschildt, P. H. 1997, ApJ, 485, 812

Nugent, P. E., Sullivan, M., Cenko, S. B., et al. 2011, Nature, 480, 344

Pereira, R., Thomas, R. C., Aldering, G., et al. 2013, ArXiv e-prints, arXiv:1302.1292

Perlmutter, S., Aldering, G., Goldhaber, G., et al. 1999, ApJ, 517, 565

Persson, S. E., Murphy, D. C., Krzeminski, W., Roth, M., & Rieke, M. J. 1998, AJ, 116, 2475

Pettini, M., & Pagel, B. E. J. 2004, MNRAS, 348, L59

Phillips, M. M. 1993, ApJ, 413, L105

Phillips, M. M., Lira, P., Suntzeff, N. B., et al. 1999, AJ, 118, 1766

Phillips, M. M., Li, W., Frieman, J. A., et al. 2007, PASP, 119, 360

Piro, A. L. 2012, ApJ, 759, 83

Piro, A. L., & Nakar, E. 2013, ApJ, 769, 67

—. 2014, ApJ, 784, 85

Prieto, J. L., Rest, A., & Suntzeff, N. B. 2006, ApJ, 647, 501

Pskovskii, Y. P. 1984, Soviet Ast., 28, 658

Rabinak, I., & Waxman, E. 2011, ApJ, 728, 63

Riess, A. G., Filippenko, A. V., Challis, P., et al. 1998, AJ, 116, 1009

Röpke, F. K., Hillebrandt, W., Schmidt, W., et al. 2007, ApJ, 668, 1132

Sahu, D. K., Tanaka, M., Anupama, G. C., et al. 2008, ApJ, 680, 580

Schlafly, E. F., & Finkbeiner, D. P. 2011, ApJ, 737, 103

Shinnaka, Y., Kawakita, H., Kobayashi, H., et al. 2013, Icarus, 222, 734

Silverman, J. M., Ganeshalingam, M., Cenko, S. B., et al. 2012, ApJ, 756, L7

Sim, S. A., Seitenzahl, I. R., Kromer, M., et al. 2013, MNRAS, 436, 333

Smith, J. A., Tucker, D. L., Kent, S., et al. 2002, AJ, 123, 2121

Stetson, P. B. 1987, PASP, 99, 191

Stritzinger, M., Mazzali, P. A., Sollerman, J., & Benetti, S. 2006, A&A, 460, 793

Stritzinger, M. D., Hsiao, E., Valenti, S., et al. 2014, A&A, 561, A146

Stritzinger, M. D., Valenti, S., Hoeflich, P., et al. 2015, A&A, 573, A2

Valenti, S., Pastorello, A., Cappellaro, E., et al. 2009, Nature, 459, 674

Wang, B., Meng, X., Liu, D.-D., Liu, Z.-W., & Han, Z. 2014, ApJ, 794, L28

Wang, X., Wang, L., Pain, R., Zhou, X., & Li, Z. 2006, ApJ, 645, 488

Wang, X., Wang, L., Zhou, X., Lou, Y., & Li, Z. 2005, ApJ, 620, L87

Wang, X., Li, W., Filippenko, A. V., et al. 2009, ApJ, 697, 380

Watanabe, M., Takahashi, Y., Sato, M., et al. 2012, in Society of Photo-Optical Instrumentation Engineers (SPIE) Conference Series, Vol. 8446, Society of Photo-Optical Instrumentation Engineers (SPIE) Conference Series

White, C. J., Kasliwal, M. M., Nugent, P. E., et al. 2015, ApJ, 799, 52

Woosley, S. E., & Weaver, T. A. 1994, ApJ, 423, 371

Yamanaka, M., Kawabata, K. S., Kinugasa, K., et al. 2009a, ApJ, 707, L118

Yamanaka, M., Naito, H., Kinugasa, K., et al. 2009b, PASJ, 61, 713

Yamanaka, M., Maeda, K., Kawabata, M., et al. 2014, ApJ, 782, L35

Yanagisawa, K., Kuroda, D., Yoshida, M., et al. 2010, in American Institute of Physics Conference Series, Vol. 1279, American Institute of Physics Conference Series, ed. N. Kawai & S. Nagataki, 466–468

Yanagisawa, K., Shimizu, Y., Okita, K., et al. 2006, in Society of Photo-Optical Instrumentation Engineers (SPIE) Conference Series, Vol. 6269, Society of Photo-Optical Instrumentation Engineers (SPIE) Conference Series

Yanagisawa, K., Shimizu, Y., Okita, K., et al. 2014, in Society of Photo-Optical Instrumentation Engineers (SPIE) Conference Series, Vol. 9147, Society of Photo-Optical Instrumentation Engineers (SPIE) Conference Series, 6

Zheng, W., Silverman, J. M., Filippenko, A. V., et al. 2013, ApJ, 778, L15

Zheng, W., Shivvers, I., Filippenko, A. V., et al. 2014, ApJ, 783, L24

TABLE 1
PROPERTIES OF SN 2012Z AND ITS HOST GALAXY NGC 1309.

SN 2012Z		References
α (2000.0)	03h22m05.35s	1
δ (2000.0)	$-15°23'15''$	1
Discovered magnitude	17.6 (Unfilter)	1
Discovery date (UT)	2012 Jan 29.150	1
Discovery date (MJD)	55955.15	1
Discoverer	Lick Observatory Supernova Search	1
SN Type	Ia-pec (Type Iax)	2,3
Galactic extinction	$E(B-V)= 0.036$	4
host galactic extinction	$E(B-V)= 0.0$	5
B-band maximum date	55965.8	5
B-band maximum magnitude	14.74 mag	5
absolude magnitude (M_B)	-17.61 mag	5
$\Delta m_{15}(B)$	1.57 ± 0.07 mag	5
v_{max}(Si II)	6980 ± 80 km s^{-1}	5
Explosion date (MJD)	55953.4 ± 0.2	5
Rise time	12.0 ± 3.0 day	5
^{56}Ni mass	$\sim 0.18\ M_{\odot}$	5
NGC 1309		
α (2000.0)	03h22m06.5s	6
δ (2000.0)	$-15°\ 24'00''$	6
morphology type	SA(s)bc	6
redshift	0.007	6
distance	29.8 ± 3.8 Mpc	6
distance modulus	32.4 ± 0.3 mag	6
apparent magnitude (B)	11.7 mag	6
absolute magnitude (M_B)	-20.65 mag	6
metallicity	$12+\log(O/H) < 8.51 \pm 0.31$	5

[1]Cenko et al. (2012c)
[2]Cenko et al. (2012a)
[3]Meyer et al. (2012)
[4]Schlafly & Finkbeiner (2011)
[5]This paper
[6]NED

TABLE 2
SUMMARY OF THE PROPERTIES OF THE TELESCOPES, INSTRUMENTS, AND OBSERVATORIES.

Observatory	Telescope	Instruments	Filters/Resolutions	Number of nights
NO[a]	1.6m Pirka	MSI[b]	U, B, V, R, I	4
AO[c]	0.5m MITSuME[d]	CCD	g', R, I	10
KAO[e]	1.3m Araki	LOSA/F2[f]	R=600	4
OAO[g]	1.88m	ISLE[h]	J, H, K_s	1
OAO	0.91m	WFC[i]	J, H, K_s	5
OAO	0.5m MITSuME[d]	CCD	g', R, I	14
NHAO[j]	2.0m Nayuta	NIC[k]	J, H, K_s	9
HHO[l]	1.5m Kanata	HOWPol[m]	B, V, R, I	23
HHO	1.5m Kanata	HOWPol	R=400	12
IO[n]	1.0m	IR Cam	J, H, K_s	12
IAO[o]	1.0m MITSuME[d]	CCD	g', R, I	7
SAAO[p]	1.4m IRSF	SIRIUS[q]	J, H, K_s	20
KO	1.88m	CCD	B, V, R, I	2
NAOJ[r]	8.2m Subaru	FOCAS[s]	B, V, R, I	1
NAOJ	8.2m Subaru	FOCAS	R=650	1

[a]Nayoro Observatory
[b]Multispectral Imager (Watanabe et al. 2012)
[c]Akeno Observatory
[d]Multicolor Imaging Telescopes for Survey and Monstrous Explosions (Kotani et al. 2005)
[e]Koyama Astronomical Obsrvatory
[f]Shinnaka et al. (2013)
[g]Okayama Astrophysical Observatory
[h]InfraRed Imager/Spectrograph (Yanagisawa et al. 2006)
[i]Wide Field Camera (Yanagisawa et al. 2014)
[j]Nishi-Harima Astronomical Observatory
[k]Nishi-harima Infrared Camera
[l]Higashi-Hiroshima Observatory
[m]Hiroshima One-shot Wide-field Polarimeter (Kawabata et al. 2008)
[n]Iriki Observatory
[o]Ishigaki-jima Astronomical Observatory
[p]South African Astronomical Observatory
[q]Near-infrared simultaneous three-band camera (Nagayama et al. 2003)
[r]National Astronomical Observatory of Japan
[s]Faint Object Camera and Spectrograph for Subaru Telescope (Kashikawa et al. 2002)

TABLE 3
LOG OF THE SPECTROSCOPIC OBSERVATIONS.

Date	MJD	Phase	Covarage	Resolution	Instruments
2012 Feb 3	55960.4	-5.0	4000-8000 Å	10.9 Å	LOSA/F2
2012 Feb 4	55961.5	-3.9	4500-9000 Å	15.0 Å	HOWPol
2012 Feb 8	55965.4	0.0	4000-8000 Å	10.9 Å	LOSA/F2
2012 Feb 9	55966.5	1.1	4500-9000 Å	15.0 Å	HOWPol
2012 Feb 11	55968.4	3.0	4500-9000 Å	15.0 Å	HOWPol
2012 Feb 11	55968.5	3.1	4000-8000 Å	10.9 Å	LOSA/F2
2012 Feb 12	55969.5	4.1	4500-9000 Å	15.0 Å	HOWPol
2012 Feb 18	55975.5	10.1	4500-9000 Å	15.0 Å	HOWPol
2012 Feb 19	55976.4	11.0	4500-9000 Å	15.0 Å	HOWPol
2012 Feb 19	55976.4	11.0	4000-8000 Å	10.9 Å	LOSA/F2
2012 Feb 20	55977.5	12.1	4500-9000 Å	15.0 Å	HOWPol
2012 Feb 26	55983.5	18.1	4500-9000 Å	15.0 Å	HOWPol
2012 Feb 27	55984.5	19.1	4500-9000 Å	15.0 Å	HOWPol
2012 Mar 11	55997.5	32.1	4500-9000 Å	15.0 Å	HOWPol
2012 Mar 13	55999.4	34.0	4500-9000 Å	15.0 Å	HOWPol
2012 Mar 15	56001.7	36.3	4500-9000 Å	15.0 Å	HOWPol
2012 Oct 23	56226.7	261.3	4600-9600 Å	9.1 Å	FOCAS

TABLE 4
Near-infrared photometry data of SN 2012Z.

MJD	J	H	$K_{\rm S}$	Instruments
55960.4	15.006(0.109)	15.334(0.270)	15.081(0.485)	NIC
55960.4	15.610(0.210)	$\cdots$	$\cdots$	WFC
55961.4	14.980(0.224)	15.079(0.217)	14.684(0.311)	NIC
55961.4	15.010(0.020)	15.210(0.030)	15.140(0.050)	ISLE
55961.5	14.931(0.037)	$\cdots$	$\cdots$	IR Cam
55961.5	15.060(0.080)	15.270(0.180)	15.130(0.280)	WFC
55961.8	14.980(0.040)	15.280(0.050)	15.160(0.100)	IRSF
55962.8	14.910(0.050)	15.030(0.050)	15.040(0.100)	IRSF
55964.8	14.620(0.050)	14.890(0.060)	14.910(0.160)	IRSF
55965.8	14.620(0.030)	14.740(0.030)	14.580(0.060)	IRSF
55966.4	$\cdots$	14.602(0.064)	14.419(0.156)	NIC
55966.5	14.659(0.030)	$\cdots$	$\cdots$	IR Cam
55966.8	14.550(0.020)	14.630(0.020)	14.620(0.060)	IRSF
55967.8	14.520(0.020)	14.610(0.020)	14.530(0.050)	IRSF
55968.4	14.411(0.031)	14.440(0.051)	14.334(0.112)	NICS
55968.4	14.520(0.050)	$\cdots$	14.250(0.090)	WFC
55968.5	14.387(0.037)	$\cdots$	$\cdots$	IR Cam
55968.8	14.430(0.020)	14.470(0.020)	14.400(0.040)	IRSF
55969.4	14.486(0.010)	14.397(0.007)	14.257(0.016)	NIC
55969.5	14.550(0.060)	$\cdots$	14.440(0.110)	WFC
55969.7	14.430(0.020)	14.410(0.020)	14.310(0.040)	IRSF
55970.7	14.430(0.020)	14.360(0.020)	14.270(0.040)	IRSF
55971.8	14.410(0.020)	14.320(0.020)	14.290(0.040)	IRSF
55972.5	14.434(0.031)	$\cdots$	$\cdots$	IR Cam
55973.5	14.348(0.033)	14.262(0.061)	$\cdots$	IR Cam
55973.8	14.430(0.020)	14.250(0.020)	14.120(0.040)	IRSF
55974.4	14.255(0.006)	14.255(0.006)	14.062(0.060)	NIC
55974.8	14.460(0.020)	14.280(0.020)	14.160(0.040)	IRSF
55975.8	14.340(0.020)	14.170(0.020)	14.130(0.040)	IRSF
55976.4	14.382(0.055)	14.094(0.072)	13.753(0.203)	NIC
55977.4	14.333(0.032)	14.055(0.014)	13.917(0.034)	NIC
55977.4	14.440(0.050)	14.230(0.070)	13.940(0.080)	WFC
55977.5	14.345(0.034)	$\cdots$	$\cdots$	IR Cam
55977.8	14.400(0.020)	14.070(0.020)	14.040(0.040)	IRSF
55983.5	14.280(0.033)	$\cdots$	$\cdots$	IR Cam
55990.8	14.380(0.030)	14.080(0.020)	14.200(0.050)	IRSF
55993.7	14.380(0.030)	14.170(0.020)	14.300(0.060)	IRSF
55995.4	$\cdots$	14.536(0.254)	$\cdots$	IR Cam
55996.4	14.705(0.030)	$\cdots$	$\cdots$	IR Cam
55996.8	14.550(0.030)	14.290(0.030)	14.320(0.060)	IRSF
55999.4	14.705(0.030)	$\cdots$	$\cdots$	IR Cam
56000.4	14.653(0.205)	$\cdots$	$\cdots$	IR Cam
56006.8	15.510(0.090)	14.730(0.060)	14.600(0.150)	IRSF
56021.7	15.960(0.120)	15.380(0.080)	16.580(0.720)	IRSF
56027.7	16.300(0.150)	15.250(0.080)	16.420(0.520)	IRSF

TABLE 5
Standard magnitudes of the comparison stars in the local field of SN 2012Z.

ID	U^a	B	g'	V	R	I	$z' + Y^b$
1	13.53 ± 0.31	13.50 ± 0.05	13.03 ± 0.02	12.77 ± 0.05	12.35 ± 0.03	11.94 ± 0.03	12.31 ± 0.01
2	13.45 ± 0.73	13.42 ± 0.05	12.85 ± 0.02	12.39 ± 0.05	11.77 ± 0.03	11.26 ± 0.03	11.56 ± 0.01
3	13.35 ± 0.18	13.32 ± 0.05	13.00 ± 0.02	12.68 ± 0.05	12.35 ± 0.03	12.07 ± 0.03	$\cdots$
4	14.25 ± 0.18	14.22 ± 0.04	13.95 ± 0.03	13.58 ± 0.04	13.27 ± 0.03	12.90 ± 0.03	13.27 ± 0.02
5	$\cdots$	16.46 ± 0.05	16.10 ± 0.06	15.89 ± 0.04	15.43 ± 0.09	15.07 ± 0.07	15.38 ± 0.06
6	$\cdots$	17.65 ± 0.09	$\cdots$	17.06 ± 0.06	16.59 ± 0.10	16.22 ± 0.07	16.22 ± 0.07
7	$\cdots$	20.21 ± 0.09	$\cdots$	18.88 ± 0.06	17.89 ± 0.10	17.06 ± 0.07	$\cdots$

[a]The U-band magnitudes were converted using the $U - B$ and $B - V$ relations in the Landolt standard magnitudes sequence (Landolt 1992). The $B - V$ color obtained via the photometric calibration with Kanata/HOWPol.

[b]The $z' + Y$-band magnitudes were calculated using the color relations between the R and $z' + Y$ bands, which were obtained from photometric calibration using the Landolt standard stars SA95 96 (Landolt 1992; Smith et al. 2002).

TABLE 6
Parameters of the optical and near-infrared light curves of SN 2012Z.

Filter	Maximum date (MJD)	Error	Maximum magnitude	Error	$\Delta m_{15}(\lambda)$	Error
B	55965.8	3.0	14.738	0.001	1.58	0.07
V	55971.8	0.20	14.470	0.008	0.75	0.05
R	55974.2	0.04	14.209	0.002	0.52	0.01
I	55977.5	0.12	13.986	0.001	0.44	0.003
J	55982.0	0.19	14.310	0.008	0.27	0.02
H	55983.9	0.04	14.027	0.002	0.32	0.01
K_s	55981.3	0.23	14.027	0.005	0.33	0.02

TABLE 7
Summary of whether the existing theoretical models are consistent with our observations.

	V_{ph}	Rise time	Spectra	LC	Luminosity
pure deflagration	YES	NO	YES	YES	YES
failed deflagration	YES	YES	YES	YES	YES
PDD	NO	YES	?	YES	YES
double detonations	NO	NO	NO	NO	NO
CC	YES	YES	?	NO	YES

TABLE 8
Optical photometry data of SN 2012Z.

MJD	U	B	g'	V	R	I	z' + Y	Instruments
55960.4	⋯	⋯	15.330(0.020)	⋯	15.130(0.020)	15.080(0.030)	⋯	MITSuME(O)
55960.5	⋯	⋯	⋯	15.273(0.230)	15.096(0.046)	15.054(0.052)	15.364(0.023)	HOWPol
55961.4	⋯	⋯	15.160(0.030)	⋯	14.930(0.020)	14.850(0.030)	⋯	MITSuME(O)
55961.4	⋯	⋯	⋯	⋯	15.181(0.029)	15.210(0.035)	⋯	MITSuME(A)
55961.5	⋯	⋯	15.125(0.004)	⋯	14.973(0.004)	15.050(0.010)	⋯	MITSuME(I)
55961.5	⋯	14.827(0.023)	⋯	14.778(0.024)	14.803(0.175)	14.700(0.175)	15.219(0.031)	HOWPol
55964.4	⋯	⋯	14.950(0.060)	⋯	14.530(0.040)	14.560(0.050)	⋯	MITSuME(O)
55964.5	⋯	14.735(0.026)	⋯	⋯	⋯	⋯	14.828(0.030)	HOWPol
55965.4	14.072(0.106)	14.922(0.012)	⋯	14.871(0.050)	14.273(0.077)	⋯	⋯	MSI
55965.4	⋯	14.832(0.049)	⋯	14.661(0.048)	14.495(0.033)	14.425(0.027)	14.736(0.039)	HOWPol
55965.4	⋯	⋯	14.738(0.047)	⋯	14.423(0.100)	14.279(0.073)	⋯	MITSuME(A)
55965.4	⋯	⋯	14.770(0.050)	⋯	14.510(0.040)	14.580(0.070)	⋯	MITSuME(O)
55966.4	⋯	14.741(0.008)	⋯	14.598(0.003)	⋯	⋯	⋯	HOWPol
55966.4	⋯	⋯	14.714(0.047)	⋯	14.385(0.117)	14.277(0.078)	⋯	MITSuME(A)
55966.5	⋯	⋯	14.720(0.030)	⋯	14.340(0.020)	14.260(0.020)	⋯	MITSuME(O)
55966.5	⋯	⋯	14.790(0.030)	⋯	14.360(0.020)	14.270(0.030)	⋯	MITSuME(O)
55968.4	⋯	14.790(0.021)	⋯	14.518(0.024)	14.322(0.025)	14.215(0.021)	14.527(0.019)	HOWPol
55968.4	⋯	⋯	14.670(0.010)	⋯	14.280(0.010)	14.240(0.010)	⋯	MITSuME(O)
55969.5	⋯	14.824(0.022)	⋯	14.506(0.042)	14.284(0.041)	14.192(0.026)	14.504(0.018)	HOWPol
55969.6	⋯	⋯	14.669(0.005)	⋯	14.300(0.005)	14.404(0.009)	⋯	MITSuME(I)
55971.5	⋯	14.942(0.026)	⋯	14.448(0.027)	14.244(0.033)	14.118(0.024)	14.431(0.019)	HOWPol
55971.5	⋯	⋯	14.667(0.003)	⋯	14.154(0.005)	14.383(0.005)	⋯	MITSuME(I)
55972.5	⋯	⋯	14.820(0.050)	⋯	14.150(0.020)	14.040(0.030)	⋯	MITSuME(O)
55973.4	⋯	⋯	14.800(0.020)	⋯	14.150(0.010)	14.040(0.020)	⋯	MITSuME(O)
55974.4	⋯	15.264(0.037)	⋯	14.500(0.030)	14.204(0.031)	14.008(0.024)	14.323(0.024)	HOWPol
55974.4	⋯	⋯	14.784(0.063)	⋯	14.159(0.101)	13.998(0.078)	⋯	MITSuME(A)
55975.4	⋯	⋯	14.870(0.020)	⋯	14.220(0.010)	13.960(0.020)	⋯	MITSuME(O)
55975.4	⋯	⋯	14.893(0.059)	⋯	14.217(0.107)	13.925(0.063)	⋯	MITSuME(A)
55975.5	⋯	15.396(0.030)	⋯	14.500(0.024)	14.211(0.028)	13.988(0.022)	14.304(0.018)	HOWPol
55976.4	⋯	15.524(0.026)	⋯	14.528(0.024)	14.208(0.028)	13.963(0.021)	14.280(0.017)	HOWPol
55976.4	⋯	⋯	14.906(0.057)	⋯	14.226(0.104)	13.901(0.068)	⋯	MITSuME(A)
55976.4	⋯	⋯	15.000(0.020)	⋯	14.220(0.010)	13.980(0.010)	⋯	MITSuME(O)
55977.4	⋯	15.653(0.030)	⋯	14.579(0.025)	14.270(0.028)	14.040(0.022)	14.356(0.019)	HOWPol
55977.4	⋯	⋯	15.090(0.060)	⋯	14.276(0.110)	13.972(0.080)	⋯	MITSuME(A)
55977.4	⋯	⋯	15.100(0.020)	⋯	14.200(0.010)	13.980(0.010)	⋯	MITSuME(O)
55977.4	⋯	⋯	⋯	14.603(0.012)	⋯	⋯	⋯	MSI
55979.4	⋯	15.844(0.019)	⋯	14.722(0.015)	⋯	⋯	⋯	MSI
55980.4	⋯	⋯	15.420(0.060)	⋯	14.286(0.110)	13.922(0.070)	⋯	MITSuME(A)
55980.5	⋯	16.171(0.382)	⋯	14.740(0.057)	14.288(0.079)	13.933(0.058)	14.253(0.077)	HOWPol
55983.4	⋯	16.690(0.039)	⋯	14.944(0.025)	14.422(0.027)	14.048(0.022)	14.369(0.066)	HOWPol
55983.4	⋯	⋯	15.670(0.050)	⋯	14.410(0.020)	14.010(0.020)	⋯	MITSuME(O)
55983.7	⋯	16.621(0.010)	⋯	15.030(0.050)	14.420(0.030)	14.010(0.030)	⋯	Kottamia
55984.4	⋯	16.774(0.044)	⋯	15.020(0.025)	14.484(0.026)	⋯	⋯	HOWPol
55984.4	⋯	⋯	15.840(0.060)	⋯	14.486(0.110)	14.042(0.070)	⋯	MITSuME(A)
55985.4	⋯	⋯	⋯	15.192(0.034)	⋯	⋯	⋯	MSI
55985.7	⋯	16.909(0.030)	⋯	15.334(0.009)	14.578(0.009)	14.153(0.013)	⋯	Kottamia
55986.5	⋯	⋯	⋯	15.234(0.041)	14.574(0.036)	14.168(0.026)	⋯	HOWPol
55987.4	⋯	⋯	16.170(0.170)	⋯	14.626(0.110)	14.212(0.080)	⋯	MITSuME(A)
55987.5	⋯	⋯	16.165(0.007)	⋯	14.648(0.004)	14.312(0.005)	⋯	MITSuME(I)
55988.5	⋯	⋯	16.195(0.034)	⋯	14.701(0.011)	14.272(0.020)	⋯	MITSuME(I)
55994.5	⋯	⋯	16.611(0.024)	⋯	15.046(0.006)	14.606(0.008)	⋯	MITSuME(I)
55996.4	⋯	⋯	⋯	15.883(0.044)	15.172(0.037)	14.648(0.028)	14.974(0.035)	HOWPol
55997.4	⋯	⋯	⋯	15.758(0.034)	15.202(0.039)	14.695(0.026)	15.020(0.021)	HOWPol
55998.4	⋯	⋯	⋯	15.807(0.038)	15.243(0.032)	14.714(0.024)	15.040(0.021)	HOWPol
55999.5	⋯	⋯	17.000(0.190)	⋯	15.220(0.030)	14.740(0.030)	⋯	MITSuME(O)
56000.5	⋯	⋯	⋯	⋯	15.282(0.060)	⋯	⋯	MITSuME(I)
56001.5	⋯	⋯	⋯	⋯	⋯	14.816(0.034)	⋯	HOWPol
56005.4	⋯	⋯	⋯	⋯	15.616(0.114)	15.025(0.067)	15.353(0.243)	HOWPol
56006.4	⋯	⋯	⋯	16.047(0.139)	15.550(0.072)	14.956(0.030)	⋯	HOWPol
56214.7	⋯	⋯	⋯	⋯	20.425(0.304)	19.625(0.217)	⋯	HOWPol
56223.4	⋯	22.062(0.070)	⋯	21.341(0.050)	21.107(0.096)	20.070(0.072)	⋯	FOCAS

APPENDIX

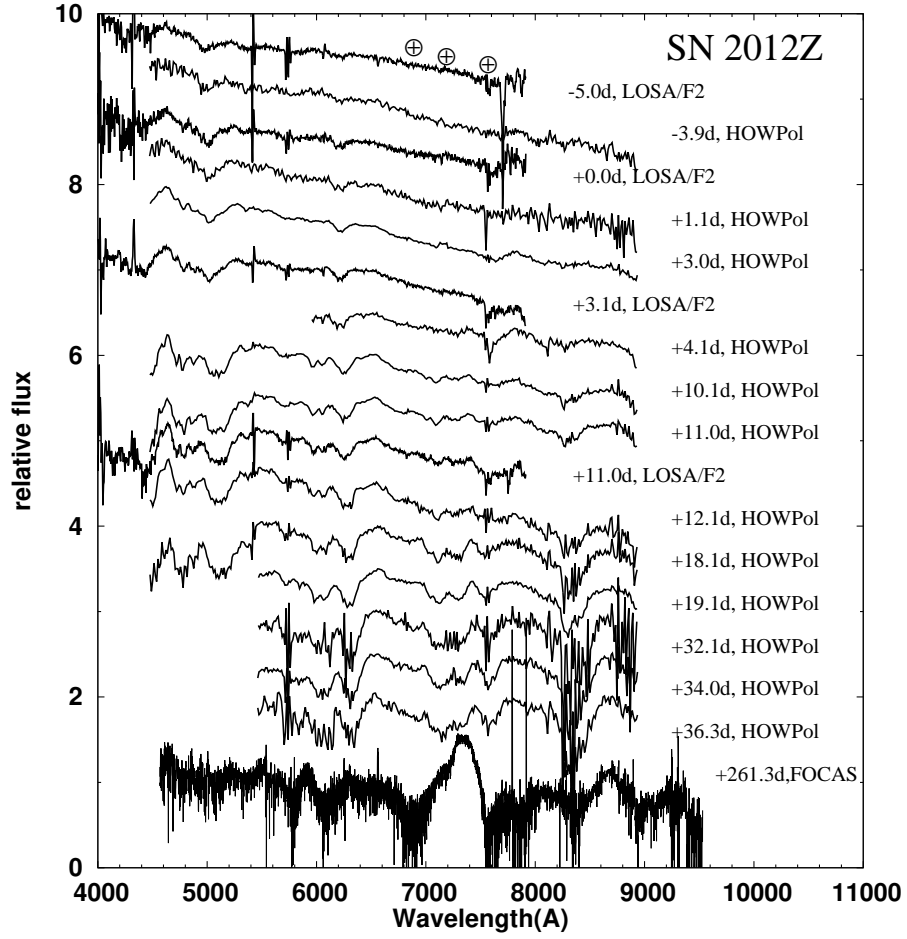OVERALL OPTICAL SPECTRAL EVOLUTIONS.

FIG. A1.— Spectral evolutions of SN 2012Z from $t = -5.1$ to 261.3 d. The absolute flux was artificially shifted. The wavelength was converted to the rest frame using z=0.007. The three symbols denote the wavelength of the atmospheric lines of the Earth.